

1 **Establishment of Proximity-dependent Biotinylation Approaches in Different Plant**
2 **Model Systems.**

3

4 **Deepanksha Arora^{1,2,*}, Nikolaj B. Abel^{3,*}, Chen Liu^{4,*}, Petra Van Damme^{1,2,5,*}, Klaas**
5 **Yperman^{1,2}, Lam Dai Vu^{1,2}, Jie Wang^{1,2}, Anna Tornkvist⁴, Francis Impens^{6,7,8}, Barbara**
6 **Korbei⁹, Dominique Eeckhout^{1,2}, Jelle Van Leene^{1,2}, Alain Goossens^{1,2}, Geert De**
7 **Jaeger^{1,2,#}, Thomas Ott^{3,10,#}, Panagiotis Moschou^{4,11,12,#}, Daniël Van Damme^{1,2,#}**

8 ¹ Ghent University, Department of Plant Biotechnology and Bioinformatics, Technologiepark
9 71, 9052 Ghent University, Ghent, Belgium.

10 ² VIB Center for Plant Systems Biology, Technologiepark 71, 9052 Ghent, Belgium.

11 ³ Faculty of Biology, Cell Biology, University of Freiburg, Germany.

12 ⁴ Department of Plant Biology, Uppsala BioCenter, Swedish University of Agricultural
13 Sciences and Linnean Center for Plant Biology, Uppsala, Sweden.

14 ⁵ Department of Biochemistry and Microbiology, Ghent University, Ghent, Belgium

15 ⁶ Department of Biochemistry, Ghent University, Ghent, Belgium.

16 ⁷ VIB Center for Medical Biotechnology, Ghent, Belgium.

17 ⁸ VIB Proteomics Core, Ghent, Belgium.

18 ⁹ Department of Applied Genetics and Cell Biology (DAGZ), University of Natural
19 Resources and Life Sciences (BOKU), Vienna, Austria.

20 ¹⁰ CIBSS – Centre for Integrative Biological Signalling Studies, University of Freiburg,
21 Germany

22 ¹¹ Department of Biology, University of Crete, Heraklion, Greece.

23 ¹² Institute of Molecular Biology and Biotechnology, Foundation for Research and
24 Technology - Hellas, Heraklion, Greece.

25

26 * joint first authors

27 # joint senior and corresponding authors

28

29 **Running title:** Proximity-dependent biotinylation in plants

30

31 The author(s) responsible for distribution of materials integral to the findings presented in this
32 article are: Geert De Jaeger (gejae@psb.vib-ugent.be), Thomas Ott (thomas.ott@biologie.uni-
33 freiburg.de), Panagiotis Moshou (Panagiotis.Moschou@slu.se) and Daniël Van Damme
34 (dadam@psb.vib-ugent.be).

35 **Abstract**

36 Proximity-dependent biotin labelling (PDL) uses a promiscuous biotin ligase (PBL) or a
37 peroxidase fused to a protein of interest. This enables covalent biotin labelling of proteins and
38 allows subsequent capture and identification of interacting and neighbouring proteins without
39 the need for the protein complex to remain intact. To date, only few papers report on the use of
40 PDL in plants. Here we present the results of a systematic study applying a variety of PDL
41 approaches in several plant systems using various conditions and bait proteins. We show that
42 TurboID is the most promiscuous variant in several plant model systems and establish protocols
43 which combine Mass Spectrometry-based analysis with harsh extraction and washing
44 conditions. We demonstrate the applicability of TurboID in capturing membrane-associated
45 protein interactomes using *Lotus japonicus* symbiotically active receptor kinases as test-case.
46 We further benchmark the efficiency of various PBLs in comparison with one-step affinity
47 purification approaches. We identified both known as well as novel interactors of the endocytic
48 TPLATE complex. We furthermore present a straightforward strategy to identify both non-
49 biotinylated as well as biotinylated peptides in a single experimental setup. Finally, we provide
50 initial evidence that our approach has the potential to infer structural information of protein
51 complexes.

52 INTRODUCTION

53 Protein-protein interaction (PPI) studies often fail to capture low-affinity interactions as these
54 are usually not maintained following cell lysis, protein extraction and protein complex
55 purification. Particularly, this is the case for PPI's of integral membrane proteins because of
56 the harsh conditions during protein extraction and purification. Proximity-dependent biotin
57 labelling (PDL) on the contrary, uses covalent biotinylation of proteins that are interactors or
58 near-neighbours of a bait protein of interest *in vivo* (Varnaite and MacNeill, 2016). Hence, to
59 identify interactions, they do not need to remain intact during purification. Although biotin is
60 an essential cofactor for a small number of omnipresent biotin-dependent enzymes involved
61 mainly in the transfer of CO₂ during HCO₃⁻-dependent carboxylation reactions, biotinylation
62 is a relatively rare *in vivo* protein modification. Moreover, biotinylated proteins can be
63 selectively isolated with high affinity using streptavidin-biotin pairing. PDL, therefore, permits
64 the identification of both high and low-affinity *in vivo* interactions.

65 Analogues to DamID in which a prokaryotic *Dam* methylase is fused to a protein of
66 interest to monitor DNA-protein interactions in eukaryotes (van Steensel and Henikoff, 2000),
67 the principle of PDL allows the capture of PPIs. More specifically, PDL is based on the fact
68 that native biotin ligases, e.g. the *Escherichia coli* BirA catalyzes a two-step reaction: first, the
69 generation of reactive biotinyl-AMP (biotinoyl-5'-AMP or bioAMP) from biotin and ATP, and
70 second, the attachment of that bioAMP to a specific lysine of the target protein. Engineered
71 PBLs have a significantly reduced affinity for the reactive bioAMP intermediate (Choi-Rhee
72 et al., 2004; Kim and Roux, 2016). This intermediate is prematurely released and, due to its
73 high reactivity, will interact with neighbouring primary amines (e.g. lysine). Therefore, these
74 variants lead to promiscuous labelling despite their lower affinity for biotin compared to native
75 biotin ligases.

76 There are several variations of PDL. The first-generation enzymes used for PDL are
77 based on the *E. coli* biotin ligase BirA (Roux et al., 2012). The mutant BirA, designated BirA*
78 (R118G) (Kwon and Beckett, 2000), referred hereafter as BioID, represents a monomeric
79 protein of 35.3 kDa, and was the first PBL variant used for PDL (Choi-Rhee et al., 2004;
80 Cronan, 2005; Kim and Roux, 2016). A second-generation PBL, called BioID2, was derived
81 from the *Aquifex aeolicus* biotin ligase (Kim and Roux, 2016). BioID2, which naturally lacks
82 a DNA-binding domain that is present in the larger BirA, is approximately one-third smaller
83 than BioID, potentially reducing sterical hindrance of the bait protein (Kim et al., 2016). The
84 third-generation PBLs, called TurboID and mini-Turbo (mTurbo), are derived from the
85 directed evolution of BirA in yeast. These two variants showed maximal activity at 30°C,

86 whereas the previous variants show maximal activity at higher temperatures (Branon et al.,
87 2018). TurboID has the same size as the original BioID tag, albeit with 14 amino acid mutations
88 that greatly increase its labelling efficiency. mTurbo has 12 out of the 14 mutations. The N-
89 terminal DNA-binding domain was deleted to reduce its size (28 versus 35 kDa), which also
90 slightly impacted on its labelling efficiency by reducing it ~2-fold. The first and second-
91 generation PBLs required approximately 18 to 24 h of labelling or sometimes even much longer
92 to produce detectable levels of protein biotinylation, while the TurboID variants required a
93 labelling time in the range of 1 h or less in the various eukaryotic, non-plant systems tested so
94 far (Branon et al., 2018).

95 PDL has its intrinsic advantages and limitations. In the presence of biotin, the bait-PBL
96 fusion protein labels proximal proteins without the activation by a conditional trigger, thereby
97 keeping track of all interactions that occurred over a time period. The ability for selective
98 capture makes the method generally insensitive to protein solubility or protein complexation,
99 with potential applicability for the interactomics studies of membrane proteins and cytoskeletal
100 constituents, providing a major advantage over alternative approaches. Nevertheless, the
101 identity of a candidate interactor does not immediately imply a direct or indirect interaction
102 with the bait but reflects merely proximity [estimated to be ~10 to 15 nm (Kim et al., 2014)].
103 Furthermore, true interactors are missed (false negatives) if they lack accessible primary
104 amines.

105 So far PBLs have successfully been used in yeast (Opitz et al., 2017b), protozoa (Opitz
106 et al., 2017a), amoebae (Batsios et al., 2016), embryonic stem cells (Gu et al., 2017), and
107 xenograft tumors (Dingar et al., 2015) to map a wide range of interactomes in both small-scale
108 (i.e. using a single bait protein) and large-scale network mapping approaches (e.g. the protein
109 interaction landscape of the centrosome-cilium interface or the organization of mRNA-
110 associated granules and bodies (mRNP complexes) (Gupta et al., 2015; Youn et al., 2018).

111 In plants, the number of reports on the use of PBLs is slowly increasing. So far, four
112 papers describe the application of the first generation of PDLs in plants (Conlan et al., 2018;
113 Das et al., 2019; Khan et al., 2018; Lin et al., 2017). In these first trials, overexpression of
114 BioID was combined with long labelling times, very high biotin levels and relatively poor
115 labelling efficiencies. These results suggest that first-generation BioID variants do not achieve
116 sufficient activity in plant tissues due to their temperature-activity profiles.

117 Recently, two studies evaluated several generations of PBLs in plants, including the
118 third generation TurboID and mTurbo using *N. benthamiana* and *Arabidopsis* seedlings as
119 model systems and concluded that TurboID outperforms the other PBLs in its capacity of both

120 *cis*- as well as specific *trans*-biotinylation of both known as well as novel target proteins under
121 conditions compatible with normal plant growth (Mair et al., 2019; Zhang et al., 2019).

122 Here, we expand our current knowledge on the use of PBL as an interactomics tool in
123 plants by performing a systematic survey of different PDL approaches in various plant systems.
124 We provide guidelines for the use of PDL in various frequently used plant models and highlight
125 the most relevant shortcomings and contingencies. Furthermore, we benchmark different PDL
126 methods at the proteomics level by studying the TPLATE protein complex and its interactors
127 using harsh extraction and washing conditions to maximize the removal of false positives. We
128 furthermore employ a strategy which allows the identification of both non-biotinylated as well
129 as biotinylated peptides from a single experiment. Finally, we provide an extensive toolkit to
130 perform PBL *in planta* and foresee that the methods, tools and materials herein will greatly
131 benefit the research community.

132

133 **RESULTS**

134 ***PBL-mediated biotin labelling efficiency increases upon biotin administration in *Solanum**** 135 ***lycopersicum***

136 In order to establish PDL in various plant systems, we first tested different PBLs in stable hairy
137 root lines of *Solanum lycopersicum* (see **Figure 1** and **Materials and Methods**). More
138 specifically, we compared the potential applicability of enzyme-catalyzed proximity labelling
139 when using BioID (Kim et al., 2016; Roux et al., 2012), BioID2 (Kim et al., 2016), TurboID
140 or mTurbo (Branon et al., 2018) as PBL. For this, we fused the engineered PBL to FLAG and
141 enhanced green fluorescent protein (eGFP) tags under control of the constitutive cauliflower
142 mosaic virus (CaMV) 35S promoter (**Supplemental Figure 1 and 2**). In all systems tested so
143 far, supplementation of biotin is important for efficient proximity biotin ligation with all the
144 PBLs tested. Plants synthesize biotin endogenously and thus, in certain systems, the
145 intracellular pool of biotin might be high enough for the PBL. In fact, free biotin accumulates
146 in plant mesophyll cells to a high concentration of ca. 11 μ M (Alban et al., 2000), while for
147 example in yeast this concentration is more than 10-fold lower (Pirner and Stolz, 2006).
148 Considering that the K_m of BioID for biotin is 0.3 μ M, this could, in theory, lead to efficient
149 PDL even in the absence of exogenous biotin supplementation.

150 We thus tested biotinylation efficiency in our hairy root system in the presence or
151 absence of biotin using different tagged PBLs as fusion proteins, either codon-optimized for
152 plants or non-codon optimized (**Supplemental Figure 1, Supplemental Table 1 and**
153 **Supplemental sequences**).

154 As a test-case for non-bait specific biotinylation, PBL-fused eGFP was used.
155 Biotinylation was evident as smears upon streptavidin-HRP-mediated Western blot detection.
156 This smear depicts biotinylation of other proteins than PBLs, and will be referred to as “*trans*-
157 biotinylation”. As a proxy of PBL activity, we used the *cis*-biotinylation efficiency (i.e. auto-
158 or self-biotinylation level of PBL fusions) as readout (**Figure 1**). Manifold faster kinetics for
159 TurboID and mTurbo over BioID and BioID2 could be observed (**Figure 1**). This is in line
160 with the previously reported lower catalytic activities of the latter PBLs, especially at the
161 growth conditions used (i.e. cultivation of hairy roots was performed at 22-25°C) (Branon et
162 al., 2018). Noteworthy, only residual *trans*-biotinylation was observed when no exogenous
163 biotin was added to the liquid grown hairy root cultures. Therefore, the addition of surplus
164 (free) biotin seems also to function as a trigger of PDL in this system. This observation
165 indicates that PDL in plants (to some extent) might also have the capacity to identify the
166 spatiotemporal dynamics of interactome composition.

167

168 ***PDL-efficiency depends on growth temperatures and PBL can facilitate trans-biotinylation*** 169 ***in Nicotiana benthamiana***

170 We used transient transformation of *Nicotiana benthamiana* leaf mesophyll cells to test the
171 applicability of PDL in a second model system commonly used for protein expression *in planta*
172 under various conditions. In this case, biotin was infiltrated directly into leaf tissue 24 h after
173 transformation and harvested 24 h post-biotin infiltration (**Supplemental Figure 3A**). We
174 confirmed that also in this system, the highest *cis*-biotinylation level was observed in case of
175 TurboID, and supplementation of biotin was important for the efficient detection of *cis*-
176 biotinylation (**Supplemental Figure 3B**). Furthermore, the overall biotinylation output signal
177 in tobacco leaves was higher when biotin concentration was increased from 50 µM to 1 mM
178 (**Supplemental Figure 3B**).

179 Evaluation of wild-type BirA showed no *trans*-biotinylation in the presence of 50 µM
180 exogenous biotin (**Supplemental Figure 4A**), confirming that the R118G mutation is
181 responsible for promiscuous labelling in plants. Furthermore, a temperature shift from 22°C to
182 28°C increased *cis*- and *trans*-biotinylation for both BioID and TurboID, suggesting that
183 temperature control can be used to modulate PDL in plants (**Supplemental Figure 4A and B**,
184 see also below).

185 Noteworthy, the effect of temperature on TurboID activity was less apparent compared
186 to that of BioID, consistent with the temperature-activity profiles of the two enzymes (Branon

187 et al., 2018). Interestingly, similar to GFP-TurboID expressed in the hairy root cultures, *cis*-
188 biotinylation (**Figure 1**), was saturating already 2 h after biotin administration in *N.*
189 *benthamiana* (**Supplemental Figure 4D**). TurboID and mTurbo were the only PBLs in plants
190 with biotinylation efficiency occurring in the range of a few hours, as other PBLs did not show
191 any visible sign of *trans*-biotinylation in that time frame (**Figure 1**).

192

193 *TurboID can be used for the efficient capture of plasma membrane interactomes in* 194 *Nicotiana benthamiana*

195 Next, we tested whether we could achieve biotinylation of protein interactors using PDL under
196 the conditions established for *N. benthamiana*. We observed that the bait proteins used in plants
197 for PDL so far were either membrane-anchored and small proteins [HopF2 (Khan et al., 2018)
198 and AvrPto (Conlan et al., 2018)], or nuclear and/or cytoplasmic localized [OsFD2 (Lin et al.,
199 2017), N (Zhang et al., 2019) and FAMA (Mair et al., 2019)].

200 We therefore tested our conditions for PDL using as test-cases, integral plasma
201 membrane-localized protein complexes with components that reside within a range of a few
202 nm. First, we used a known membrane receptor complex from *Lotus japonicus* comprising two
203 symbiotically active receptor-like kinases (RLK): the LysM-type RLKs NOD FACTOR
204 RECEPTOR 5 (NFR5) and the LRR-RLK SYMBIOTIC RECEPTOR-KINASE (SYMRK).
205 These proteins assemble within the same complex in *L. japonicus* roots (Ried et al., 2014) as
206 well as in *N. benthamiana* upon heterologous expression (Antolin-Llovera et al., 2014). In
207 contrast, the brassinosteroid receptor BRASSINOSTEROID INSENSITIVE 1 (BRI1) did not
208 co-immunoprecipitate with the symbiotic receptor complex indicating no or only weak
209 interactions with these RLKs (Antolin-Llovera et al., 2014). However, using Bimolecular
210 Fluoresce Complementation (BiFC), another study reported some interactions between NFR5
211 and BRI1 as well as with the *A. thaliana* innate immune pattern recognition receptors
212 FLAGELLIN SENSING 2 (FLS2) (Madsen et al., 2011). To further extend the set of control
213 proteins, we additionally included the EF-TU RECEPTOR (EFR), belonging to the LRR-
214 family, as well as the LOW TEMPERATURE INDUCED PROTEIN LTI6b that is commonly
215 used as a plasma membrane marker in plant cell biology (Grebe et al., 2003).

216 In a first experiment, we tested whether cytosolic TurboID would non-specifically
217 *trans*-biotinylate the receptors at the plasma membrane. For this, we co-expressed a TurboID-
218 GFP fusion protein with GFP-tagged receptors in *N. benthamiana* and immunoprecipitated (IP)
219 all components using an anti-GFP nanotrap (**Supplemental Figure 5A**). While all co-
220 expressed proteins could be detected before and after the IP, we only detected *cis*-biotinylation

221 of TurboID-GFP but not of the receptors (**Supplemental Figure 5A**). This indicates the
222 absence of non-specific *trans*-biotinylation of membrane resident receptors by a soluble
223 TurboID itself. However, it should be clearly stated that prolonged reaction times and increased
224 expression of TurboID will likely result in a certain degree of non-specificity due to the
225 inherent features of the system.

226

227 To test biotinylation between membrane-resident receptors, we co-expressed a NFR5-
228 TurboID (120 kDa) fusion protein with either the known NFR5-interacting RLK SYMRK or
229 with BRI1 and FLS2 that may not be stable components of the NFR5/SYMRK receptor
230 complex. As higher degrees of non-specificity are expected for proteins that reside in close
231 proximity with each other, we tested *trans*-biotinylation 15 and 30 minutes after addition of
232 exogenous biotin (**Figure 2 and Supplemental Figure 5**). As expected, we observed weak
233 *trans*-biotinylation of SYMRK-GFP (150 kDa) by NFR5-TurboID after 15 minutes when
234 SYMRK-GFP was immunoprecipitated using anti-GFP nanotrap beads. With 30 minutes
235 labeling time, stronger *trans*-biotinylation of SYMRK5-GFP was detected (**Figure 2**, upper
236 panel). When applying the same experimental conditions to plants co-expressing BRI1-GFP
237 (157 kDa) and NFR5-TurboID, we detected no *trans*-biotinylation after 15 minutes and only
238 very weak *trans*-biotinylation after 30 minutes of BRI1-GFP. These data show that temporal
239 control during labelling experiments is crucial to maintain specificity in the system, and that
240 BRI1 may reside in close proximity to the NFR5/SYMRK complex, despite a lack of a stable
241 and physical interaction.

242 Given these results, we sought to test a number of other membrane proteins to elucidate
243 whether the observed levels of non-specificity are at least partially dependent on the target
244 protein. We co-expressed NFR5-TurboID with the transmembrane proteins FLS2, EFR and
245 LTI6b. While no *trans*-biotinylation of EFR and LTI6b was detected, we observed a weak
246 signal for BRI1 as shown above as well as for FLS2, but again considerably lower compared
247 to the levels found for SYMRK, indicating an important impact of the target proteins on the
248 *trans*-biotinylation patterns (**Supplemental Figure 5B**). It should be noted that we were not
249 able to detect *cis*-biotinylated NFR5 after immunoprecipitating SYMRK using GFP-nanotraps.
250 This is most likely due to the stringent washing conditions and the possibility that only a
251 fraction of NFR5-TurboID was co-immunoprecipitated together with SYMRK. Taken
252 together, these data are in line with a previously published report (Madsen et al., 2011) and
253 show that predominant *trans*-biotinylation of proximal membrane-resident proteins is possible,
254 even under constitutive expression in heterologous systems. However, stringent control of

255 experimental conditions such as expression levels and exposure time to biotin is greatly
256 advised.

257 In summary, these data clearly show that TurboID-mediated PDL can be efficiently
258 used for capturing interactors of membrane proteins. Furthermore, it can be advantageous over
259 other methods such as co-immunoprecipitation as it does not require any optimization of the
260 solubilization conditions and provides the possibility to detect transient protein complex
261 constituents.

262

263 *Application of PDL in Arabidopsis thaliana cell cultures using the TPLATE complex as a* 264 *case study*

265 Next, we surveyed the efficiency of *trans*-biotinylation for a stable multi-subunit plant protein
266 complex. As a test case, we selected the plasma membrane-associated octameric TPLATE
267 complex (TPC) (Gadeyne et al., 2014) and used stably transformed *A. thaliana* cell suspension
268 cultures as a third plant model system for PDL.

269 Given the higher biotinylation level observed in *N. benthamiana* at 28°C
270 (**Supplemental Figure 4**), we started with evaluating different labelling conditions. To study
271 the temperature effect in this system, we grew cells expressing TPLATE-BioID and GFP-
272 BioID, i.e. proteins fused to the first generation PBL, at various temperatures in the presence
273 of 50 µM biotin for 24 h. We subsequently isolated the complex under non-denaturing
274 conditions using streptavidin affinity purification (see **Materials and Methods**), performed
275 tryptic on-bead digest and analyzed the released non-biotinylated peptides using LC-MS/MS.

276 In order to evaluate the effect of temperature on the biotinylation efficiency and on the
277 subsequent identification of the proteins from the isolated complexes, we focused on the other
278 seven TPLATE complex members. We compared their abundances and fold changes to the
279 control setup (35S::GFP-BioID) after streptavidin purification, taking into account label-free
280 protein quantification (LFQ) intensities (Cox et al., 2014) (**Figure 3A**). In addition to the bait,
281 all seven interacting subunits could be significantly detected at all tested temperatures (**Figure**
282 **3B, Supplemental Data Set 1**). The fold changes observed with respect to the control were
283 however not dramatically different between the different temperatures. As we did not observe
284 any major differences with respect to the efficiency of detecting TPC subunits at all tested
285 temperatures, and given the increased efficiency observed in *N. benthamiana* at 28 °C and the
286 likely negative impact of increased temperature on the physiology of the plants, we opted for

287 28°C as an optimal trade-off to perform a series of follow-up experiments on the TPC in *A.*
288 *thaliana* cultures.

289

290 ***Various PBLs affect biotinylation of TPC subunits differently***

291 The introduction of a flexible linker (Roux et al., 2012) has been successfully used to extend
292 the labelling radius of PBLs (Kim et al., 2016) (Kim et al., 2016), which is estimated to be
293 about 10 to 15 nm (Kim et al., 2014). This increased labelling radius may be desirable when
294 the protein of interest is significantly larger than the labelling radius of the PBL alone, and/or
295 when the goal is to map the constituency of a larger protein complex or a discrete subcellular
296 region. We thus compared the efficiencies of various PBLs and assessed their biotinylation
297 radius by inserting a 65 aa long flexible linker. *Arabidopsis* cultures expressing C-terminal
298 fusions of TPLATE with BioID or BioID2 were assessed, with and without a 65 aa linker
299 similar to the one that was reported before (Roux et al., 2012). As controls, we generated GFP
300 fused to BioID or BioID2 without additional linker (**Supplemental Figure 6**).

301 To test the effect of the linker and to further evaluate the activity of different PBLs in
302 *Arabidopsis* cell culture, transgenic cultures were grown for 24h, with and without exogenous
303 biotin at 28°C, and expression and biotinylation were assessed via Western blotting
304 (**Supplemental Figure 6**). Protein abundance of the BioID and BioID2 constructs was
305 comparable to their respective controls in our cell cultures and was not affected by the addition
306 of biotin. Only TPLATE-BioID2 levels were rather lower. At the level of *cis*- and *trans*-
307 biotinylation, we observed different patterns for each of the fusion proteins used. As several of
308 the detected bands which increased significantly in the presence of biotin, did not correspond
309 to bands in the control or GFP-BioID culture and varied between the different PBLs, they likely
310 represent different *trans*-biotinylated interactors and suggest that the outcome of a BioID-based
311 interaction assay might partially depend on the PBL used. TPLATE-linker PBL showed the
312 most complex biotinylation pattern when comparing to the other setups expressing BioID and
313 BioID2 fusions (**Supplemental Figure 6**), suggesting that the addition of a linker may be used
314 to enhance proximity labelling. Consistent with the results described for tobacco, TurboID
315 constructs showed some residual biotinylation without the addition of exogenous biotin,
316 increased biotinylation after 1 h incubation with biotin and gave rise to an extensive
317 biotinylation pattern after 24 h incubation with biotin in both control and bait cultures,
318 suggesting it is highly promiscuous.

319 As observed in *N. benthamiana* (**Supplemental Figure 3**) using GFP as bait protein,
320 BioID also outperformed BioID2 using TPLATE as bait in this system, although this might (in
321 part) be skewed due to the lower expression levels of the latter. Adding a flexible linker
322 increased *cis*-biotinylation levels of the bait compared to the constructs without linker
323 (**Supplemental Figure 6A and C**). Overall, our results are consistent with previous
324 observations in non-plant systems suggesting that linkers increase the biotinylation output
325 (Kim et al., 2016).

326 Following the positive effect of exogenous biotin supplementation (**Supplemental**
327 **Figures 3 and 4**), we tested the effect of increasing biotin concentrations on *cis*-biotinylation
328 efficiency. Cell cultures expressing TPLATE-linkerBioID were grown at 28°C in the presence
329 of increasing concentrations of biotin (50 µM to 4 mM) for 24 hours and analyzed by Western
330 blotting (**Supplemental Figure 7A**). Supplementing the culture with biotin concentrations in
331 the range of 50 µM to 2 mM increased *cis*-biotinylation output up to ~2-fold. Increasing biotin
332 concentration >2 mM did not further increase *cis*-biotinylation efficiency (**Supplemental**
333 **Figure 7B**).

334 We took advantage of the increased biotinylation observed by including a long linker
335 sequence and generated *Arabidopsis* cultures expressing GFP-linkerTurboID and TPLATE-
336 linkerTurboID. Similar to other reports, when sampling was done 24 h post-biotin addition,
337 TurboID efficiency strongly outperformed all other PBLs tested as evident from the high
338 biotinylation levels observed with and without the addition of exogenous biotin for both the
339 control (GFP) as well as the TPLATE expressing cultures (**Supplemental Figure 6B and D**).

340 In order to compare the different PBL modules, we processed the isolated proteomes of
341 our cell cultures for LC-MS/MS analysis and focused on the relative levels of the various TPC
342 subunits compared to the control setup. Our first mass spectrometry results following
343 streptavidin purification under non-denaturing conditions and on-bead digestion identified all
344 known subunits of the TPC (**Figure 3**). Given that TPC is a robust multi-subunit complex
345 (Gadeyne et al., 2014) and that we identify only non-biotinylated peptides with our on-bead
346 digestion protocol, we assumed that the subunits we detect are a combination of direct
347 biotinylation as well as co-immunoprecipitation of the complex as a whole under the non-
348 denaturing conditions. To test this, we adapted our protocol (**Figure 4A**) and performed protein
349 extraction and stringent washing steps under denaturing conditions using a buffer containing
350 8M urea and 2% SDS to unfold proteins before streptavidin immunoprecipitation and to
351 remove non-specific, or indirect, non-biotinylated protein binders. We also included the

352 TPLATE-linkerBioID setup treated with 2 mM biotin for 24 h to assess if increased biotin
353 concentration improves TPC subunit detection.

354 In agreement with the higher stringency of the isolation procedure, the smallest TPC
355 subunit, LOLITA, which was robustly detected using AP-MS (Gadeyne et al., 2014) and, as
356 shown here, without being denatured before binding to streptavidin beads (**Figure 3**), was no
357 longer detected (**Figure 4B, Supplemental Data Set 2**). LFQ revealed that the remaining seven
358 TPC subunits, including the bait TPLATE, were detectable using BioID, linkerBioID,
359 linkerBioID2 and linkerTurboID, although not all subunits were significantly enriched
360 compared to the GFP PBL control using our statistical threshold criteria (FDR 0.05 and S0 of
361 0.5). The TASH3 and TWD40-2 subunits, for example, could not be confidently identified with
362 all PBLs. For BioID2, this might be caused by the reduced expression level of the bait in these
363 cultures (**Supplemental Figure 6**), yet this does not explain why this low level of detection is
364 not observed for the other subunits as well (**Figure 4**). We also conclude that adding a long
365 linker increased the robustness of prey identification. For example, using TPLATE-
366 linkerBioID, the TASH3 subunit was detected with 15 peptides compared to only 2 peptides
367 when using TPLATE-BioID (**Supplemental Table 3**). We did not identify TASH3 with
368 TPLATE-BioID2, in contrast to TPLATE-linkerBioID2, where we identified TASH3 with 59
369 peptides (**Supplemental Table 3**).

370 Noteworthy, increasing the concentration of biotin from 50 μ M to 2 mM adversely affected
371 TPC subunit detection as only the bait itself could be identified. It is likely that increasing
372 biotin concentrations causes residual free biotin to accumulate in the protein extract, even after
373 protein desalting to deplete free biotin, thereby occupying the streptavidin binding sites on the
374 beads which are saturated at $>9 \mu$ M of biotin. We tested this “saturation hypothesis” using *N.*
375 *benthamiana* leaves and protein precipitation to completely remove residual biotin, showing
376 that even at low concentration, residual biotin can saturate the streptavidin beads and
377 incapacitate detection (**Supplemental Figure 8**). Hence, special care should be taken to avoid
378 an excess of residual free biotin during streptavidin-based capture. A similar conclusion was
379 obtained in other studies combining PBL with MS analysis *in planta* (Mair et al., 2019; Zhang
380 et al., 2019).

381 It should be noted that the fold change by which the other TPC subunits were detected
382 with TurboID was comparable or sometimes even lower (e.g. AtEH2/Pan1) compared to the
383 other BioID forms tested (**Figure 4**). This was caused by the fact that TPC subunits were
384 identified with higher abundance in the TurboID control samples, resulting in lower relative

385 fold changes. All individual TPC subunits were detected with more than 20 unique peptides
386 using the GFP-linkerTurboID whereas TWD40-2 was the only TPC subunit detected in the
387 other control GFP-PBLs, which explains its overall low fold change (**Supplemental Table 3**).
388 Nevertheless, TurboID identified most of the TPC subunits more robustly compared to the
389 other PBLs, as evidenced by the overall higher $-\log_{10}p$ -values. So, although in our case,
390 TurboID showed to be superior to all others in identifying the other TPC subunits, the lower
391 signal/noise ratio of TurboID, due to its increased activity, might work as a disadvantage to
392 observe differences between bait proteins and control samples, which might even be enhanced
393 if the proteins are targeted to specific subcellular locations.

394

395 *The structural composition of protein complexes causes differences in detection between* 396 *PDL and AP-MS*

397 To further evaluate PDL, we compared the relative levels compared to the bait by which the
398 different TPC subunits were detected using PDL using our stringent washing protocol with a
399 one-step IgG-based pull-down (PD) protocol using the GS^{rhino} tandem affinity purification
400 (TAP) tag (Van Leene et al., 2019). To do this, we used the Maxquant iBAQ value, which is
401 the result of the summed intensity values of the identified peptides, divided by the number of
402 theoretical peptides. We calculated these iBAQ values for each TPC subunit, normalized it to
403 the value for the bait (TPLATE) to correct for differences in bait fusion expression levels, and
404 compared the values of TPLATE-linkerBioID, TPLATE-linkerBioID2 and TPLATE-
405 linkerTurboID with those from PD. When normalized to the bait protein (TPLATE), the other
406 TPC subunits are detected by TurboID at similar levels as compared to PD (**Figure 5A,**
407 **Supplemental Data Set 3**). The one exception is the subunit LOLITA, which could only be
408 detected by PD. The six other TPC subunits could also be significantly detected by BioID and
409 BioID2, however with less efficiency.

410 The fact that the smallest subunit, LOLITA, could only be identified via AP-MS, indicates that
411 this subunit is not biotinylated although it harbors 11 lysine residues, possibly reflecting the
412 structural composition of the TPC. Our results furthermore reveal that, except for LOLITA, all
413 TPC subunits, which are part of a protein complex in the range of 1MDa can be identified using
414 our stringent wash protocol as a proxy for biotinylation.

415

416 *TurboID allows broadening the interactome of protein complexes*

417 We subsequently broadened the analysis towards other interactors and compared all proteins
418 that were significantly enriched in one of the datasets (TPLATE-GS^{rhino}, TPLATE-

419 linkerBioID, TPLATE-linkerBioID2 and TPLATE-linkerTurboID) (**Supplemental Table**
420 **4A**). Whereas the overall number of significant interactors identified with the GS^{rhino} and
421 linkerBioID tags was higher than the number of significant interactors found with
422 linkerTurboID, the latter identified several known players in clathrin-mediated endocytosis
423 (CME) with much stronger statistical significance (**Figure 5A**). These players included the two
424 Clathrin Heavy Chains (CHC), and several Dynamin Related Proteins (DRP). Moreover,
425 TPLATE-linkerTurboID allowed to significantly enrich for novel interactors with a clear link
426 to CME such as the Secretary Carrier Membrane Protein 5 (SCAMP5) and an ANTH/ENTH
427 protein, PICALM3. Integral membrane SCAMP proteins are hypothesized to act in both the
428 exo- and endocytic pathways between the PM and TGN (Law et al., 2012). PICALM3
429 (Phosphatidylinositol binding clathrin assembly protein) was not identified before as a TPC
430 interactor, but PICALM4A (AtECA4) and 4B (CAP1), were previously found associated with
431 TPC (Gadeyne et al., 2014) and also confirmed here using our PD approach (**Figure 5A**).

432

433 ***Identification of biotinylated peptides enhances the identification power of PDL and allows***
434 ***identifying structural relationships between complex subunits***

435 The interaction between biotin-streptavidin is strong enough to be maintained even under harsh
436 conditions (**Supplemental Figure 8**). Thus, biotinylated peptides are expected to be retained
437 on the streptavidin beads. Following stringent washing under denaturing conditions, on-bead
438 digest will release non-biotinylated proteins, which can subsequently be identified using LC-
439 MS/MS. This approach, however, does not provide direct evidence for biotinylation and it
440 relies on the assumption that only biotinylated proteins remain bound to the beads after the
441 washing steps. To acquire direct proof of biotinylation, and to further enhance the power of
442 PDL to identify interactors, release of biotinylated peptides from the Streptavidin beads and
443 their subsequent MS-based identification is required.

444 Thus, we expanded the protocol (**Figure 5B**) to also be able to identify biotinylated
445 peptides. For this, we included a second elution step (see **Materials and Methods**) to release
446 the biotinylated peptides from the beads using an adapted protocol based on previous work
447 (Schiapparelli et al., 2014). This approach enables the detection of both non-biotinylated as
448 well as biotinylated peptides in the same experimental setup.

449 As a previous report on TurboID describes no major changes in the activity of TurboID
450 between 22 and 30°C and used biotin treatments of only a few hours (Mair et al., 2019), we
451 tested whether we could improve the identification of novel TPC interactors by reducing the
452 time of biotin addition to our cell cultures grown at normal growth temperatures. We, therefore,

453 performed a series of experiments comparing short (10min and 1h), medium (6 h) and long (24
454 h) biotin treatments at the normal growth temperature (25°C) of our *Arabidopsis* cell culture.
455 We compared the iBAQ values of all significant hits, using both elutions of each experiment
456 at 25°C with those from our 24hrs experiment at 28°C (**Figure 5B** and **Supplemental Table**
457 **4B**). The robustness of detecting interactors clearly increased with longer biotin incubation
458 times. Also, there was a positive effect of working at a slightly elevated temperature (**Figure**
459 **5C**). Combining both elution fractions also increased the robustness of interactor identification.
460 More specifically, including the second elution allowed the identification of additional DRPs,
461 AtECA4 as well as TOL6 and TOL9 (**Figure 5C**), compared to the results when only the first
462 elution (on-bead digestion) was analysed (**Figure 5A**).

463 Out of the five TOL proteins studied so far, TOL6 and TOL9 localize strongly at the plasma
464 membrane (Moulinier-Anzola et al., 2020). TOL proteins are part of the endosomal sorting
465 complexes required for transport (ESCRT) pathway and act as gatekeepers for degradative
466 protein sorting (Korbei et al., 2013). We confirmed the association between TPLATE and
467 TOL6, TOL9 and SCAMP5. TOL6-Venus revealed a high degree of colocalization with
468 TPLATE-TagRFP at endocytic foci on the PM (**Figure 6A**), which was severely reduced when
469 the image of one channel was flipped horizontally (**Figure 6B**). Furthermore, quantitative
470 analysis showed TPLATE interacting with TOL9 and SCAMP5 by ratiometric BiFC. The
471 YFP/RFP ratio was significantly higher for all four independent combinations tested compared
472 to a control set where we combined TPLATE with the shaggy-like kinase BIN2 (**Figure 6C** to
473 **6H**). The identification and confirmation of these novel interactors shows that PDL can expand
474 our knowledge on the interactomes of multisubunit complexes in plants beyond currently used
475 AP-MS-based approaches.

476
477 Next to enhancing the robustness of TurboID to identify interactors, the identification of
478 biotinylated peptides also provides direct proof of the proximity of specific domains of the prey
479 proteins with respect to the bait. We, therefore, tested whether biotinylated peptides could
480 reveal differential proximity between specific domains of TPC subunits using the TPLATE-
481 linkerTurboID as bait (**Figure 7** and **Supplemental Data Set 4**). The highest number of
482 biotinylated peptides were identified for TPLATE (44 biotinylated peptides), followed by
483 TWD40-1 (18), AtEH2/Pan1 (16), AtEH1/Pan1 (12), TWD40-2 (9) and TML (3). No
484 biotinylated peptides could be detected for LOLITA, correlating with our previous results.
485 Mapping non-biotinylated and biotinylated peptides, taking into account their relative
486 abundance, on the different TPC subunits revealed differences in the number of detected

487 peptides as well as differences in the distribution of the biotinylated peptides along the length
488 of the subunits. Whereas the bait, TPLATE, shows a relatively even distribution of biotinylated
489 peptides along the protein sequence, there is a clear tendency of the AtEH1/Pan1, AtEH2/Pan1
490 and TML subunits towards increased biotinylation at their C-terminal parts (**Figure 7**). It is
491 tempting to speculate that the observed distribution of biotinylated peptides, as well as their
492 absence, reflect the proximity of the domains as well as structural constraints with respect to
493 the bait protein and that proximity biotinylation, next to providing topology information in case
494 of transmembrane proteins (Kim et al., 2018), also harnesses the potential to help deduce
495 structural insight into protein complexes.

496

497 **DISCUSSION**

498 We provide a comprehensive comparison of various PBL based proximity labelling strategies
499 in plants. We show that TurboID is the most promiscuous PBL, and that this sometimes leads
500 to a lower signal to noise ratio. We also provide guidelines and approaches for interactome
501 capture in various plant systems specifically focusing on proteins that are intrinsic or peripheral
502 to the plasma membrane. Furthermore, we show that for each bait/system conditions might
503 benefit from independent optimization.

504 We observed that in all three plant systems tested, the exogenous application of biotin
505 enhances PDL output but might not be a strict requirement for the successful application of
506 PDL. This result seems to contradict with what has been reported for a related method called
507 INTACT (isolation of nuclei tagged in specific cell types) in plants. This method allows for
508 affinity-based isolation of nuclei from individual cell types of tissue. INTACT relies on the
509 endogenous pool of biotin as no exogenous supplementation is required (Deal and Henikoff,
510 2011). In INTACT, nuclei are affinity-labelled through transgenic expression of the wild-type
511 variant of BirA which biotinylates a nuclear envelope protein carrying biotin ligase recognition
512 peptide from ACC1. This tag acts as a native substrate for the *E. coli* biotin ligase BirA (Beckett
513 et al., 1999). The use of wild-type BirA along with its preferable substrate could explain the
514 higher affinity for the free biotin pool in INTACT, and the peptide used as fusion is an optimal
515 substrate for the bioAMP intermediate. We assume that various proteins may show variability
516 in functioning as acceptors of bioAMP (e.g. depending on the accessibility of lysine residues).

517 PDL utilizing bacterial enzymes poses the question of whether these enzymes could
518 perform adequately in plants (Kim et al., 2016). The activity optimum for BioID2 is 50°C,
519 whereas for BioID this is 37°C and thus BioID2 may be most adequate for use at higher
520 temperature conditions. Both temperatures are however far-off from the usual growth

521 temperatures of most plant species grown in temperate regions (e.g. several *Arabidopsis* sp.).
522 Both BioID2 and BioID show reduced activity below 37°C [(Kim et al., 2016) and our results
523 herein]. Furthermore, the lower temperature optimum of TurboID (and mTurbo) (Branon et al.,
524 2018) would imply that TurboID may function better at normal plant growth temperature.
525 Previous work showed no enhanced activity of TurboID when using temperatures above
526 normal plant growth conditions (Mair et al., 2019). We observed however that TurboID
527 activity increases around 2-fold from 22°C to 28°C and that there is a beneficial effect of
528 slightly increasing the growth temperature of our cell cultures on the identification of specific
529 interactors of TPC. At all tested temperatures, we observed that TurboID (and mTurbo)
530 outperforms other PBLs in terms of speed and promiscuity. Hence, TurboID might be preferred
531 over other pBLs when it concerns the initial study of (transient) complex composition where
532 the generation of as much as possible specific biotinylation output in a short time might be
533 desirable.

534 However, the strong promiscuity of the control might also work as a disadvantage in
535 revealing specific interactions in cases where the reaction cannot be controlled that easily in
536 time or when both the bait and the control would be targeted to a confined intracellular space.
537 Furthermore, controls may express at high levels and show increased diffusion due to their
538 smaller hydrodynamic radius, further skewing results.

539 We provide evidence that our methods and conditions apply to plasma-membrane
540 complexes. We showed that the interaction of the symbiotic RLKs NFR5 and SYMRK can be
541 identified by exploiting PDL and particularly the PBL TurboID. Furthermore, the use of proper
542 negative controls is imperative. However, even though the brassinosteroid receptor BRI1 was
543 not co-immunoprecipitated with the symbiotic receptors in a previously published dataset
544 (Antolin-Llovera et al., 2014), we detected weak biotinylation of this RLK and the immune-
545 receptor FLS2. While it could be interpreted as unspecificity within the PBL system, it should
546 also be considered, that PBL allows labelling of transient interactions or proximal proteins. As
547 a consequence, continuous unstable interactions accumulate to detectable amounts of proteins
548 and would thus allow their identification. As PDL using TurboID is capable of *trans*-
549 biotinylation in the range of minutes (15 min under our experimental conditions), the
550 enrichment of unstable interactions would thus be more prominent. Therefore, putative
551 interactions identified by PBL still need to be verified using independent experimental systems
552 but comparisons between the different experimental systems should always reflect the technical
553 limitations of each approach.

554 By expanding our protocols and PBLs into *Arabidopsis* cell cultures, we could not only
555 reproduce the composition of the TPC except for one subunit, but we could also robustly
556 identify and confirm other CME players and novel interactors using the third generation PBL.
557 We show that MS-based identification of interactors is more robust using prolonged biotin
558 exposure of *Arabidopsis* cell cultures and that the use of linkers can be advantageous when it
559 comes to identifying protein-protein interactions of multi-subunit complexes. Furthermore,
560 TPLATE-linkerBioID2 shows reduced *cis*-biotinylation compared to TPLATE-linkerBioID in
561 the presence of exogenous biotin but seems to function in the absence of biotin suggesting that
562 in plants, BioID2 can function in tissues where exogenous supplementation of biotin may be
563 less effective, e.g. the vasculature. Furthermore, increased biotin application can lead to serious
564 impediments when it comes to the identification of interactors as this can interfere with
565 biotinylated proteins binding on streptavidin slurries. Caution is warranted to assure sufficient
566 capture-capacity of biotinylated proteins since the amount of beads needed for capture should
567 be tested for each experimental model system/setup/protocol.

568 Complementary to the reports on TurboID *in planta* published so far (Mair et al., 2019;
569 Zhang et al., 2019), we have established a strategy that uses much harsher conditions, with
570 higher concentrations of SDS and urea for extraction and washing to remove as much as
571 possible false positives (i.e. non-biotinylated proteins). Finally, we also provide a protocol for
572 the simultaneous identification of biotinylated and non-biotinylated peptides. This approach
573 allowed us to increase the robustness of interactor identification and provided evidence for the
574 accessibility of different protein domains to PDL. We show that AtEH1/Pan1, AtEH2/Pan1
575 and TML subunits are preferentially biotinylated at their C-terminal parts, suggesting that their
576 C-termini are in closer proximity to the C-terminal end of TPLATE and/or some domains (even
577 complex subunits such as LOLITA) are not accessible for biotinylation. We thus provide
578 evidence that PDL approaches in plants, combined with harsh extraction/washing conditions
579 may be able to provide structural information of multi-subunit protein complexes and that this
580 may be extended to the topology of membrane proteins.

581 Our results are complementary to the work deposited in BioRxiv reporting the use of
582 TurboID to identify transient signalling components (Kim et al., 2019) and novel regulators of
583 plant immunity (Zhang et al., 2019), as well as for the efficient capturing of cell- and
584 subcellular compartment-specific interactomes (Mair et al., 2019). Taken together, these four
585 studies provide a new arena for the identification of novel protein-protein interactions in plants.
586

587 MATERIAL AND METHODS

588 *Bacterial strains*

589 For cloning, *Escherichia coli* strains DH5 α , DH10B or Top10 were used using standard
590 chemical transformation protocols. Electrocompetent *Agrobacterium tumefaciens* C58C1 Rif^R
591 (pMP90), AGL1 Rif^R or GV3101 Rif^R bacterial cells (i.e. a cured nopaline strain commonly
592 used for tobacco infiltration (Ashby et al., 1988) were used for tobacco infiltration as well as
593 Arabidopsis cell culture transformation. Electrocompetent rhizogenic *Agrobacterium* (RAB)
594 ATCC15834 (ATCC® 15834™)(Kajala et al., 2014) bacterial cells were used for hairy root
595 transformation.

596

597 *Cloning of constructs*

598 For constructs used in hairy roots: Constructs encoding the full-length ORF of the PBL
599 (e.g. BioID (pDEST-pcDNA5-BioID-Flag C-term, a kind gift from the Gingras laboratory
600 (Couzens, Knight et al. 2013)), BioID2 (MCS-BioID2-HA, Addgene, Plasmid #74224 (Kim,
601 Jensen et al. 2016)), TurboID (V5-TurboID-NES_pCDNA3, Addgene, Plasmid #107169
602 (Branon, Bosch et al. 2018)), mTurbo (V5-miniTurbo-NES_pCDNA3, Addgene, Plasmid
603 #107170 (Branon et al., 2018) were PCR amplified using Q5® High-Fidelity DNA Polymerase
604 (New England Biolabs, Cat n° M0491) with oligonucleotide primers containing attB
605 recombination sequences. The forward and reverse primer additionally encoded the GGGGS
606 linker and the Flag-tag (DYKDDDDK) followed by a stop codon, respectively. The primer
607 sequences are depicted in **Table S2**. The resultant attB-flanked PCR products were used in a
608 Gateway® BP recombination reaction with the pDONR™ P2r-P3 vector (Life Technologies,
609 Carlsbad, CA, USA) according to the manufacturer's instructions, thereby creating an entry
610 clone. The construct was transformed in DH5 α chemical competent cells and verified by
611 sequencing (i.e. Sanger sequencing). Using a standard multisite (3-fragment) Gateway® LR
612 cloning strategy as described by (Van Leene et al., 2007), the entry clones together with pEN-
613 L1-F-L2 encoding eGFP (Karimi et al., 2007a) (<https://gateway.psb.ugent.be/search>) and pEN-
614 L4-2-R1 encoding the constitutive cauliflower mosaic virus (CaMV) 35S promoter (Karimi et
615 al., 2007a), were recombined with the multisite Gateway destination vector pKm43GW
616 (Karimi et al., 2007a) to generate expression constructs. More specifically, the multisite LR
617 Gateway reaction resulted in translational fusions between the eGFP and the proximity labels,
618 driven by the 35S promoter. This way, the following expression constructs were created;
619 Pro35S::eGFP-BioID, Pro35S::eGFP-BioID2, Pro35S::eGFP-TurboID and Pro35S::eGFP-

620 miniTurbo and Pro35S::eGFP-BioID construct (in pKm43GW), with a C-terminally triple HA-
621 tagged BioID fused to eGFP.

622 For constructs used in *N. benthamiana*: original BioID, BioID2 and TurboID DNA
623 sequences were taken from (Branon et al., 2018; Kim et al., 2014; Roux et al., 2012), codon-
624 optimized to *Arabidopsis*. The GOLDENGATE compatible BirA, BioID, BioID2 and TurboID
625 were synthesized and codon-optimized using the codon optimization tool of Integrated DNA
626 Technologies, Inc. The ORFs were synthesized with BsaI overhangs and were ligated to the
627 Level1/2 vector pICSL86900 and pICSL86922, as previously described (Patron et al., 2015).
628 The following expression vectors were used: Pro35S::BirA-Myc, Pro35S::BioID-myc,
629 Pro35S::HF-BioID2-HA and Pro35S::superfolderGFP-TurboID-FLAG.

630 The genomic sequence of NFR5 and the coding sequence of BRI1 was synthesized with
631 BsaI overhangs for Golden Gate as Level1 vector (Binder et al., 2014). Pro35S::NFR5-
632 TurboID and Pro35S::BRI1-GFP were created by Golden Gate cloning in Xpre2-S
633 (pCAMBIA) vectors (Binder et al 2014). Pro35S::FLS2-GFP was kindly provided by Hemsley
634 lab, University of Dundee, Scotland. Pro35S::EFR-GFP (Schwessinger et al., 2011) and
635 Pro35S::SymRK-GFP/ Pro35S::NFR5-GFP (Madsen et al., 2011; Wong et al., 2019) were
636 kindly provided by Cyril Zipfel (University of Zurich, Switzerland) and Jens Stougaard
637 (Aarhus University, Denmark).

638 BiFC constructs were created in the 2in1 BiFC vectors (Grefen and Blatt, 2012). The
639 entry clones were generated by a Gateway® BP recombination reaction using coding sequences
640 of SCAMP5 and TOL9 (BioXP/gBlocks, IDT). TPLATE was amplified from the pDONR
641 plasmid described before (Gadeyne et al., 2014). All entry clones were sequence verified. The
642 BIN2 entry plasmid was kindly provided by Jenny Russinova (Houbaert et al., 2018). Entry
643 clones were combined in a Gateway® LR recombination reaction with an empty BiFC
644 destination vector and selected using LB containing spectinomycin and Xgal. Final BiFC
645 vectors were checked by restriction digest and sequencing of the recombination borders.

646 For constructs used in *A. thaliana*: BioID and BioID2 DNA sequences were taken from
647 (Kim et al., 2014; Roux et al., 2012), codon-optimized for *Arabidopsis* using the codon
648 optimization tool of Integrated DNA Technologies, Inc. The BioID and BioID2 with and
649 without linker (GGGGS)₁₃ with stop codon, flanked by attB2 and attB3 sites (Karimi et al.,
650 2005) were synthesized by Gen9 in the Gm9-2 plasmid. The TurboID sequence (Tess et al.,
651 2018) was codon-optimized to *Arabidopsis* using the codon optimization tool of Integrated
652 DNA Technologies, Inc. TurboID with linker (GGGGS)₁₃ with stop codons, flanked by attB2
653 and attB3 sites (Karimi et al., 2005), was synthesized by GenScript in the pUC57 plasmid.

654 Entry clones of eGFP (Mylle et al., 2013), and TPLATE (At3g01780) (Van Damme et al.,
655 2006) without stop codon were used in a triple Gateway LR reaction, combining pK7m34GW
656 or pH7m34GW (Karimi et al., 2005), pDONRP4-P1R-Pro35 and pDONRP2-P3R-
657 BioID/BioID2/(GGGGS)₁₃BioID/(GGGGS)₁₃ BioID2/(GGGGS)₁₃ TurboID to yield
658 pK7m34GW, Pro35S::GFP/TPLATE-BioID, pK7m34GW, Pro35S::GFP, pH7m34GW,
659 Pro35S::TPLATE-BioID2, pK7m34GW, Pro35S::TPLATE-(GGGGS)₁₃ BioID/BioID2 and
660 pK7m34GW, Pro35S::GFP/TPLATE-(GGGGS)₁₃ TurboID. Sequences of these constructs can
661 be found in supplementary data.

662 ProTOL6p::TOL6:Ven was obtained by replacing mCherry in
663 ProTOL6::TOL6:mCherry (Korbei et al., 2013) with the Venus-tag (Ven), which was PCR
664 amplified with the primer pair: NotImcherryu/NotImcherryd from proPIN2::PIN2:VEN
665 (Leitner et al., 2012).

666

667 ***Plant transformations***

668 Hairy roots: Seeds of tomato (*Solanum* spp.) cv. Moneymaker were surface-sterilized in 70%
669 ethanol for 10 min and in 3% NaOCl for 20 min (rinsing with sterile deionized water was
670 performed in between the two sterilization steps), and then rinsed 3 times 5 min each with
671 sterile deionized water. The seeds were germinated on Murashige and Skoog (MS) tissue
672 culture medium (Murashige and Skoog, 1962) containing 4.3 g/L MS medium (Duchefa;
673 catalog no. M0221.0050), 0.5 g/L MES, 20 g/L sucrose, pH 5.8, and 8 g/L agar (Difco; catalog
674 no. 214530) in magenta boxes (~50 ml). The pH of the medium was adjusted to 5.8 with KOH
675 and autoclaved at 121°C for 20 min. The boxes were covered and placed in the dark at 4°C in
676 a cold room for two days. Subsequently, the boxes were transferred to a 24°C growth chamber
677 (16 h light/8 h photoperiod) for ~10 days until cotyledons were fully expanded and the true
678 leaves just emerged. Rhizogenic *Agrobacterium* (RAB) transformation was essentially
679 performed as described previously (Harvey et al., 2008) with some minor modifications. More
680 specifically, competent rhizogenic *Agrobacterium* cells were transformed by electroporation
681 (Shen and Forde 1989) with the desired binary vector, plated on YEB medium plates with the
682 appropriate antibiotics (100 mg/L spectinomycin), and incubated for 3 to 4 d at 28°C. A
683 transformed rhizogenic *Agrobacterium* culture was inoculated from fresh plates into YEB
684 liquid medium with the appropriate antibiotics added and grown overnight at 28°C with
685 shaking at 200 rpm. The RAB culture was used to transform 20 to 40 tomato cotyledon halves.
686 Using a scalpel, the cotyledons were cut in half from ~10 days old tomato seedlings, transferred
687 (adaxial side down) onto MS liquid medium. The MS liquid was subsequently removed and

688 the cotyledon halves immediately immersed in a bacterial suspension at an optical density at
689 600 nm of 0.3 in MS liquid medium for 20 min, then blotted on sterile Whatman filter paper
690 and transferred (adaxial side down) onto MS agar plates without antibiotics (4.3 g/L MS
691 medium, 0.5 g/L MES, 30 g/L sucrose, pH 5.8, and 8 g/L agar). The co-cultivation culture
692 plates were sealed with aeropore tape. After 3 to 4 days of incubation at 22-25°C in the dark
693 (Oberpichler, Rosen et al. 2008), the cotyledons were transferred to MS agar plates with 200
694 mg/L cefotaxime (Duchefa; catalogue no. c0111.0025) and 50 mg/L kanamycin and returned
695 to 22-25°C. Typically, three to five independent roots arise from each cotyledon. The
696 expression of the eGFP marker of antibiotic-resistant roots that emerged was monitored by
697 using fluorescent microscopic imaging (Leica stereomicroscope and imaging DFC7000 T
698 Leica microscope camera) and four to ten independent roots showing expression of the marker
699 were subcloned for each construct. These roots were subsequently transferred to new selection
700 plates with the same antibiotic concentration for 3 rounds of subcultivation (~6 weeks) before
701 antibiotics-free cultivation of the hairy root cultures in liquid MS (in 50 ml Falcon tubes
702 containing 10 to 30 ml MS medium at 22-25°C and shaking at 300 rpm) and downstream
703 analysis. After 3 rounds of cultivation, root cultures were maintained and grown in antibiotics-
704 free half-strength ($\frac{1}{2}$) MS medium supplemented with 3% sucrose at 22-25°C.

705 *N. benthamiana*: Wild-type tobacco (*Nicotiana benthamiana*) plants were grown under normal
706 light and dark regime at 25°C and 70% relative humidity. 3- to 4-weeks old *N. benthamiana*
707 plants were watered from the bottom ~2h prior infiltration. Transformed *Agrobacterium*
708 *tumefaciens* strain C58C1 Rif^R (pMP90), AGL1 Rif^R or GV3101 Rif^R harbouring the
709 constructs of interest were used to infiltrate tobacco leaves and used for transient expression of
710 binary constructs by *Agrobacterium tumefaciens*-mediated transient transformation of lower
711 epidermal leaf cells essentially as described previously (Boruc et al., 2010). Transformed
712 *Agrobacterium tumefaciens* were grown for ~20h in a shaking incubator (200 rpm) at 28°C in
713 5 mL of LB-medium (Luria/Miller) (Carl Roth) or YEB medium, supplemented with
714 appropriate antibiotics (i.e. 100 g/L spectinomycin). After incubation, the bacterial culture was
715 transferred to 15 ml Falcon tubes and centrifuged (10 min, 5,000 rpm). The pellets were washed
716 with 5 mL of the infiltration buffer (10 mM MgCl₂, 10 mM MES pH 5.7) and the final pellet
717 resuspended in the infiltration buffer supplemented with 100-150 μ M acetosyringone. The
718 bacterial suspension was diluted with supplemented infiltration buffer to adjust the inoculum
719 concentration to a OD₆₀₀ value of 0.025-1.0. The inoculum was incubated for 2-3 h at room
720 temperature before injecting and delivered to tobacco by gentle pressure infiltration of the

721 lower epidermis leaves (fourth and older true leaves were used and about 4/5-1/1 of their full
722 size) with a 1-mL hypodermic syringe without needle (Moschou et al., 2016).

723 Arabidopsis cell suspension: The PSB-D Arabidopsis thaliana cell suspension cultures were
724 transformed with the POI: Pro35S::GFP/TPLATE/TML-BioID/BioID2,
725 Pro35S::TPLATE/TML-(GGGGS)₁₃ BioID/BioID2 and Pro35S::GFP/TPLATE-(GGGGS)₁₃
726 TurboID and selected without callus screening, grown and subcultured as described by (Van
727 Leene et al., 2007).

728 Arabidopsis plants to express TOL6-Venus: Flowering *tol2-1/tol2-1 tol5-1/tol5-1 tol6-1/tol6-1*
729 *1 tol9-1/tol9-1* plants were transformed with *Agrobacterium tumefaciens* using the floral dip
730 method (Clough and Bent, 1998). Resulting T2 lines were confirmed for single-transgene
731 insertion sites and propagated for further analysis. At least three independent transformants
732 were characterized for each line. Homozygous plants were confirmed by PCR genotyping for
733 the mutant alleles (Korbei et al., 2013).

734 ***Biotin treatments***

735 *Hairy roots*: For assessing self-biotinylation, 2 weeks old 25 ml liquid cultures were added 5
736 ml fresh MS medium with or w/o supplemented biotin (i.e. 50 µM f.c.; stock solution dissolved
737 in water) for 2h or 24h and samples collected. Two independent root cultures were analyzed
738 per combination and the experiment repeated twice with similar results.

739 *N. benthamiana* leaves: Plants were kept under normal growing conditions 22°C, re-infiltrated
740 with infiltration buffer (no biotin) or alternatively, infiltration buffer supplemented with biotin
741 (stock solution dissolved in DMSO or water) and samples collected at the indicated times
742 points. Two infiltrated tobacco leaf segments/leaves were analyzed per combination.

743 *Arabidopsis* cell cultures: were grown under normal conditions, at 25°C at 130 rpm in the dark.
744 48 h after subculturing, the required amount of biotin was added and the cell culture was
745 transferred to the desired temperature for the required time at 130 rpm shaking in the dark in
746 an INCLU-line IL56 (VWR) incubator. After the needed time, cell cultures were harvested and
747 flash-frozen in liquid nitrogen and stored at -70° till used.

748

749 ***Protein extractions***

750 *Hairy roots*: The tissue samples were flash-frozen and crushed using a liquid cooled mortar and
751 pestle and the crushed material was transferred to a 1.5 ml Eppendorf in homogenization buffer

752 (25 mM Tris-HCl pH 7.6, 15 mM MgCl₂, 5 mM EGTA, 150 mM NaCl, 15 mM
753 pNO₂PhenylPO₄, 15 mM β-glycerolphosphate, 1 mM DTT, 0.1% NP-40, 0.1 mM Na₃VO₄, 1
754 mM NaF, 1 mM PMSF, 10 μg/ml leupeptin, 10 μg/ml aprotinin, 10 μg/ml SBTI, 0.1 mM
755 benzamidine, 5 μg/ml antipain, 5 μg/ml pepstatin, 5 μg/ml chymostatin, 1 μM E64, 5% ethylene
756 glycol) was added with volumes according to the dry weight of the recovered material (1/1
757 w/v) and protein material extracted by three repetitive freeze-thaw cycles in liquid nitrogen and
758 the lysate transferred to a 1.5 ml Eppendorf. The lysates were cleared by centrifugation for 15
759 min at 16,100 x g (4 °C) and the supernatant transferred to a new 1.5 ml Eppendorf. This step
760 was repeated two times and the protein concentration was determined by the DC Protein Assay
761 Kit (Bio-Rad, Munich, Germany) according to the manufacturer's instructions.

762 *N. benthamiana* leaves: The tissue samples were crushed using a liquid cooled mortar and
763 pestle and the crushed material transferred to a 1.5 ml Eppendorf in homogenization buffer.
764 Leaves were harvested and directly frozen in liquid nitrogen. Proteins were extracted with
765 buffer containing 50 mM Tris-HCl (pH 7.5), 150 mM NaCl, 10 % glycerol, 2 mM EDTA, 5
766 mM DTT, 1 mM PMSF, Protease inhibitor Cocktail (Roche) and 1 % (v/v) IGEPAL CA-630
767 (Sigma-Aldrich). Extraction buffer was added at 2 ml/g tissue. Extracts were incubated at 4 °C
768 for 1 h and then centrifuged at 4 °C, 13000 rpm for 30min. Supernatants were used directly or
769 filtered through PD-10 columns (GE Healthcare) and incubated with streptavidin (Roche) or
770 GFP (Chromotek) beads for 1 h. For ammonium acetate protein precipitation, supernatants
771 were precipitated using 5x v/v pre-cold 0.1 M ammonium acetate in methanol at -20 °C for 2h
772 and then centrifuged at 4 °C, 13,000 rpm for 15min. The pellet was washed with pre-cold 0.1
773 M ammonium acetate and dissolved in the same extraction buffer plus 1% SDS. Magnetic
774 separation was done using Dynabeads™ M-280 Streptavidin (Thermo Fisher Scientific)
775 followed by 5 times washing in buffer containing 50 mM Tris-HCl (pH 7.5), 150 mM NaCl,
776 10 % glycerol, 2 mM EDTA, Protease inhibitor Cocktail (Roche) and 0.5 % (v/v) IGEPAL
777 CA-630 (Sigma-Aldrich) and one time in buffer containing 50 mM Tris-HCl (pH 7.5), 1M
778 NaCl, 10 % glycerol, 2 mM EDTA, Protease inhibitor Cocktail (Roche) and 0.5 % (v/v)
779 IGEPAL CA-630 (Sigma-Aldrich) at 4°C. To release the proteins, 100 μl 2x NuPAGE LDS
780 sample buffer (Invitrogen) was added and samples were heated for 5 min at 95 °C

781 *Arabidopsis cell cultures*: Total protein extracts were obtained from biotin treated, harvested
782 and liquid nitrogen retched (20 Hz, 1 min), *Arabidopsis* cell suspension cultures using double
783 the volume (w/2v) of extraction buffer containing 150 mM Tris-HCl pH 7.5; 150 mM NaCl;
784 10 % glycerol; 10 mM EDTA; 1mM sodium molybdate; 1 mM NaF and freshly added 10 mM

785 DTT; 1 % (v/v) protease inhibitor cocktail (P9599, Sigma (1 tablet/10ml elution buffer) and
786 1 % (v/v) NP-40. Cell debris was removed by two rounds of centrifugation at 14,000 rpm for
787 20 min at 4°C and the supernatant was collected.

788 ***SDS-PAGE and Western blots***

789 *Hairy roots*: Sample loading buffer was added and equivalent amounts of protein (~ 30 µg)
790 separated by SDS-PAGE (1.0 mm thick 4 to 12% polyacrylamide Criterion Bis-Tris XT- gels,
791 Bio-Rad or equivalent) in MOPS buffer (Bio-Rad) at 150 V. Subsequently, proteins were
792 transferred onto PVDF membranes with 0.2 µm porous size. Membranes were blocked for 30
793 min in a 1:1 Tris-buffered saline (TBS)/Odyssey Blocking solution (cat n° 927-40003, LI-
794 COR, Lincoln, NE, USA) and probed by Western blotting. Following overnight incubation of
795 primary antibody in TBS-T/Odyssey blocking buffer and three 10 min washes in TBS-T (0.1%
796 Tween-20), membranes were incubated with secondary antibody for 30 min in TBS-T/Odyssey
797 blocking buffer followed by 3 washes in TBS-T or TBS (last wash step). The following
798 antibodies were used: streptavidin-S680 (Invitrogen, S32358, 1/10000), mouse anti-Flag
799 (Sigma, F3165; 1/5000), mouse anti-actin (plant) (Sigma, A0480, 1/2000), rabbit anti-GFP
800 (Invitrogen, A11122, 1/1000), anti-mouse (IRDye 800 CW goat anti-mouse antibody IgG, LI-
801 COR, cat n° 926-32210, 1/10000) and anti-rabbit (IRDye 800 CW goat anti-rabbit IgG, LI-
802 COR, cat n° 926-3221, 1/10000). The bands were visualized using an Odyssey infrared
803 imaging system (LI-COR) and the intensity of bands assessed using the LICOR Odyssey
804 software for Western Blot image processing.

805 *N. benthamiana*: Extracted proteins were loaded to 12% SDS-PAGE gels and separated for 2
806 h at 90-110V. SDS-PAGE gels were blotted via wet transfer on PVDF membranes (Carl Roth)
807 overnight at 30V. Membrane blocking was performed with 3% BSA in PBS-t buffer for 1 h at
808 room temperature followed by incubation with Mouse-anti-GFP (TaKaRa) (1/5,000) for 2 h
809 followed by Anti-Mouse-HRP (Sigma-Aldrich) (1/5,000) for 2 h or directly Strep-Tactin-HRP
810 (iba-Life Sciences) (1/5,000) for 2 h. Chemiluminescence was detected with Clarity Western
811 ECL (Bio-rad).

812 *N. benthamiana*: Input and eluted proteins were loaded to 12% SDS-PAGE gels and separated
813 for 1-2 h at 120 V. SDS-PAGE gels were blotted via wet transfer on PVDF membranes (Bio-
814 rad) 3h at 300 mA in a cool room. The membrane was blocked with 3% BSA in PBS-T buffer
815 for 1 h at room temperature followed by incubation with Streptavidin-HRP (Sigma-Aldrich)

816 (1/25,000) for 2 h. Chemiluminescence was detected with ECL Prime Western Blotting
817 Detection Reagent (GE healthcare).

818 *Arabidopsis cell cultures*: The total protein extracts were heated in sample buffer for 10 min at
819 70°C and loaded in equal amounts (20 µg, protein concentration was measured using a qubit
820 system, ThermoFischer) on a 4-20% SDS-PAGE gel. SDS-PAGE separated proteins were
821 blotted on PVDF membrane (Thermo Fisher). Membranes were blocked overnight at RT in 5%
822 (v/v) BSA dissolved in 25 mM Tris-HCl, pH 8, 150 mM NaCl and 0.1% Tween20. The blots
823 were then incubated at room temperature with the Pierce High Sensitivity Streptavidin-HRP
824 Thermo Fisher scientific (1/2,000) or Abcam Anti-HA-HRP tag antibody (ab1190) (1/5,000)
825 in 1% BSA made as mentioned above for 2 h. Antigen-antibody complexes were detected using
826 chemiluminescence (Perkin-Elmer).

827

828 *Imaging analysis*

829 A *tplate* mutant complemented line expressing proLAT52::TPLATE-TagRFP (Wang et al.,
830 BioRxiv 948109) was crossed with a quadruple *tol* (*tol2/tol2 tol5/tol5 tol6/tol6 tol9/tol9*)
831 mutant line expressing proTOL6::TOL6-Venus. F1 seedlings were imaged using spinning discs
832 microscopy. Etiolated hypocotyl cells of 4-day old seedlings expressing TPLATE-TagRFP and
833 TOL6-Venus were imaged with a Nikon Ti microscope equipped with an Ultraview spinning-
834 disk system (PerkinElmer) and a 512 x 512 Hamamatsu ImagEM C9100-13 EMccd camera.
835 Images of hypocotyl epidermal cells were acquired with a 100x oil immersion objective (Plan
836 Apo, NA = 1.45). TOL6-Venus was imaged with 514 nm excitation light and an emission
837 window between 525 nm and 575 nm. TPLATE-TagRFP was imaged with 561 nm excitation
838 light and an emission window between 570nm and 625nm. Dual-color images were acquired
839 sequentially with an exposure time of 500 ms/frame.

840

841 Objects based co-localization was performed using the plugin Distance Analysis (DiAna) of
842 ImageJ (Gilles et al., 2017). Prior to analysis with the DiAna plugin, images were processed
843 with ImageJ. Each channel is processed using a Walking Average of 4 and then merged (also
844 rotated if required). Regions of interest within each image were selected based on that they
845 excluded the border of the cells and still contained a good number of objects. Z-projection
846 images were generated using five frames with average intensity. Then, each channel of Z-
847 projected images was processed with Morphological filters from the MorphoLibJ plugin
848 (Legland et al., 2016), using the parameters white top-hat, disk element and a 2 pixel radius.

849 Objects for each channel were segmented by selecting the 3D Spot segmentation tool. We
850 adapted the calibration by changing the pixel size to 1.00001 for all dimensions. Both the noise
851 and seed threshold value were obtained by averaging the maximum intensity of three regions
852 covering only background signal. The spot was defined using a minimum value of 4 and
853 maximum value of 36 pixels. The option to exclude objects on XY edges was activated. Default
854 values were used for the other parameters. Results for number of total objects (Tot) or touching
855 objects (Tou) in image A/B obtained from Diana were recorded. The colocalization ratio of
856 objects was calculated as follows:

857
$$\text{only (A)\%} = (\text{Tot A} - \text{Tou A}) / ((\text{TouA} + \text{TouB}) / 2 + (\text{Tot A} - \text{Tou A}) + (\text{Tot B} - \text{Tou B})) * 100\%$$

859
$$\text{only (B)\%} = (\text{Tot B} - \text{Tou B}) / ((\text{TouA} + \text{TouB}) / 2 + (\text{Tot A} - \text{Tou A}) + (\text{Tot B} - \text{Tou B})) * 100\%$$

860
$$\text{Cocolcalization\%} = 100\% - \text{only (A)\%} - \text{only (B)\%}$$

861 As a control, one of the channels was horizontally flipped, merged with the other channel and
862 analyzed. 8 cells originating from 3 seedlings were analyzed.

863

864 ***Bimolecular Fluorescence Complementation***

865 Ratiometric BiFC images were obtained using an Olympus FV1000 inverted confocal
866 microscope equipped with a UPLSAPO 60x water immersion objective (NA 1.2). Images were
867 acquired in line sequential mode, using 515 nm excitation and an emission window between
868 530 nm to 548 nm for the YFP detection and using 559 nm excitation and an emission window
869 between 580 nm to 615 nm for RFP detection. All images were taken using the exact same
870 settings. The experiment was independently repeated twice with similar outcome.

871 For the quantification of the YFP/RFP ratio, only images with less than 1% saturation in the
872 RFP or YFP channel were analysed. For each confocal image, parts of the cortical cytoplasm
873 in the RFP channel were traced in ImageJ using the selection brush tool with a width of 15
874 pixels. Histogram analysis was performed to confirm that less than 1% saturated pixels were
875 present in the ROI. The average intensity from the obtained ROI was calculated and divided
876 by the average intensity of the same region in the YFP channel. Ratios were quantified for 15
877 to 19 individual cells.

878 Outliers were removed by iterative outlier removal (Leys et al., 2013). Data were analyzed
879 using Rstudio (RStudio Team (2015). RStudio: Integrated Development for R. RStudio, Inc.,
880 Boston, MA URL <http://www.rstudio.com/>) with Welch-corrected ANOVA to account for
881 heteroscedasticity. Post hoc pairwise comparison was performed with the package
882 MULTCOMP utilizing the Tukey contrasts (Herberich et al., 2010).

883

884 ***Protein Extraction and Pull down for Mass Spectrometry analysis***

885 For Figure 3: *Arabidopsis* cell cultures expressing different POI were ground in 0.67 volume
886 of extraction buffer containing 150 mM Tris-HCl pH 7.5; 150 mM NaCl; 10 % glycerol; 10
887 mM EDTA; 1mM sodium molybdate; 1 mM NaF and freshly added 10 mM DTT; 1 % (v/v)
888 protease inhibitor cocktail (P9599, sigma (1 tablet/10ml elution buffer), 1 % (v/v) digitonin
889 and benzonase 0.1% (w/v). The extract was mixed using ultra-Turrax for 3x30" at 16000 rpm
890 and sonicated for 15"x 3 with 30" interval. The extract was incubated on a rotating wheel for
891 1 hour at 4°C. Cell debris was removed by two rounds of centrifugation at 20,000 rpm for 20
892 mins at 4°C and the supernatant was buffer exchanged using pre-equilibrated PD-10 columns
893 and eluted in binding buffer (extraction buffer without digitonin and benzonase) at 4° C. Pull-
894 downs were performed in triplicate. For each pull-down, 1/3 of the soluble protein extract was
895 incubated with 200 µl slurry of streptavidin sepharose high-performance beads (Amersham)
896 (pre-equilibrated with binding buffer) overnight on a rotating wheel at 4°C. The unbound
897 fraction or supernatant, was removed after centrifugation at 1,500 rpm for 1 min. Beads were
898 transferred to a mobicol column and washed with 2.5 ml binding buffer followed by wash with
899 2.5 ml of wash buffer-1 containing 25mM Tris-HCl (pH7.5); 150mM NaCl; digitonin 0.1%
900 (w/v). The beads were washed once with wash buffer-2 containing 25mM Tris-HCl pH7.5; 150
901 mM NaCl and finally washed once with 50 mM ammonium bicarbonate pH 8.0. Proteins were
902 digested on beads with Trypsin/LysC (Promega) overnight followed by zip-tip cleanup using
903 C-18 Omix tips (Agilent). Digests containing the unbiotinylated peptides were dried in a
904 speedvac and stored at -20 °C until LC-MS/MS analyses.

905 For Figure 4 and Figure 5: *Arabidopsis* cell cultures expressing different POI were ground in
906 0.67 volume of extraction buffer containing 100 mM Tris (pH 7.5), 2% SDS and 8M Urea. The
907 extract was mechanically disrupted using three repetitive freeze-thaw cycles followed by 2
908 cycles of sonication at output level 4 with a 40% duty cycle for 50" with 35" interval. The
909 extract was incubated at rotating wheel for 1 hour at RT. Cell debris was removed by two
910 rounds of centrifugation at 20,000 rpm for 20 mins at RT and the supernatant was buffer
911 exchanged using pre-equilibrated PD-10 columns and eluted in binding buffer containing 100
912 mM Tris (pH 7.5), 2% SDS and 7.5M Urea. Pull-downs were performed in triplicate. For each
913 pull-down, 1/3 of the soluble protein extract was incubated with 200 µl slurry of streptavidin
914 sepharose high-performance beads (Amersham) (pre-equilibrated with binding buffer)
915 overnight on a rotating wheel at RT. The unbound fraction or supernatant, was removed after

916 centrifugation at 1,500 rpm for 1 min. Beads were transferred to a mobicol column and washed
917 with 4 ml binding buffer for 5 mins without agitation, followed by a wash with high salt buffer
918 containing 1M NaCl, 100 mM Tris-HCl pH 7.5 and incubated for 30 mins. The beads were
919 washed once with ultrapure water, incubated for 5 mins and finally washed with 3.2ml of 50
920 mM ammonium bicarbonate pH 8.0 incubating 5 mins. Proteins were digested on beads with
921 Trypsin/LysC (Promega) overnight followed by zip-tip cleanup using C-18 Omix tips
922 (Agilent). Digests containing the unbiotinylated peptides were dried in a Speedvac as elution-
923 1 (E1) and stored at -20 °C until LC-MS/MS analyses.

924 After E1, for all linkerTurboID samples, biotinylated peptides were eluted from the beads, by
925 adding 300µl of the elution buffer containing 0.2% TFA, 0.1% formic acid and 80% acetonitrile
926 in water. The eluted peptides were collected by centrifugation at 1500 rpm for 1 min followed
927 by an addition to the beads of 300µl of the elution buffer, after which the sample was heated at
928 95°C for 5 min to allow a maximal release of peptides. A short spin at 1,500 rpm for 1 min was
929 done to collect the eluted peptides. The two elutes were pooled and dried in a speedvac. The
930 dried peptides were dissolved in 1% TFA solution to perform zip-tip cleanup using C-18 Omix
931 tips (Agilent). Digests were dried in a speedvac as elution-2 (E2) and stored at -20 °C until LC-
932 MS/MS analysis.

933 TPLATE-CGSrhino pull-downs with home-made IgG beads were performed as described in
934 (Van Leene et al., 2019).

935

936 ***Mass Spectrometry and Data Analysis***

937 Triplicate pull-down experiments were analyzed by LC-MSMS on Q Exactive (ThermoFisher
938 Scientific) as previously reported (Nelissen et al., 2015).

939 For comparison of TPLATE-BioID at 25, 28, 30 and 35 degrees, raw data of GFP-BioID and
940 TPLATE-BioID triplicates at the different incubation temperatures were searched together
941 with MaxQuant (Tyanova et al., 2016a) using standard parameters (Supplemental Dataset 1).
942 LFQ intensities were used in Perseus software (Tyanova et al., 2016b) to determine the
943 significantly enriched proteins with TPLATE for each sample set, TPLATE versus GFP at
944 respectively 25, 28, 30 and 35 degrees. Thereto the MaxQuant proteingroups file, with reverse,
945 contaminant and only identified by site identifications already removed, was loaded in Perseus.
946 Samples were grouped by the respective triplicates and filtered for minimal 2 valid values per
947 triplicate. Missing LFQ values were imputed from normal distribution using standard settings
948 in Perseus, width of 0.3 and down shift of 1.8. Next, ttests were performed and visualized in
949 volcano plots, using permutation-based FDR to determine the significantly different proteins

950 between TPLATE-BioID and GFP-BioID at the different incubation temperatures. As cut-off,
951 FDR=0.05, S0=0.5 was applied. Protein lists significantly enriched with TPLATE can be found
952 in Supplemental Table 4. For all TPC subunits, the values for Difference and $-\log(p\text{-value})$
953 from the Perseus t-test were presented in Figure 3, in order to compare the different TPLATE-
954 BioID samples and determine the optimal temperature for BioID.

955 For comparison of different TPLATE PBLs at 28 degrees, triplicate TPLATE-BioID,
956 TPLATE-BioID2, TPLATE-linkerBioID, TPLATE-linkerBioID2, TPLATE-linkerTurboID
957 and respective controls GFP-BioID, GFP-BioID2 and GFP-linkerTurboID raw data was
958 searched together in MaxQuant with standard parameters (Supplemental
959 Table 5). Datasets were further processed in the same way as described for the comparison of
960 the different incubation temperatures. GFP-BioID served as control for TPLATE-BioID and
961 TPLATE-linkerBioID, and GFP-BioID2 served as control for TPLATE-BioID2 and TPLATE-
962 linkerBioID2. For linkerBioID, next to 50 μ M biotin incubation, also 2mM biotin incubation
963 was tested. Pairwise comparisons were made between the different TPLATE PBLs and their
964 respective controls, and a cut-off of FDR=0.05, S0=0.5 was applied. Protein lists significantly
965 enriched with TPLATE can be found in Supplemental Table 5. For all TPC subunits, the values
966 for Difference and $-\log(p\text{-value})$ from the Perseus ttests were presented in Figure 4, in order to
967 compare the different TPLATE PBLs. TPLATE-CGSrhino pull-downs were analyzed as
968 described in Van Leene et al., 2019. Briefly, pull down triplicates were analyzed by LC-MSMS
969 on Q Exactive (ThermoFisher Scientific), raw data were searched with the Mascot search
970 engine (Matrix Science) and average Normalized Spectral Abundance Factors (NSAF) for the
971 identified proteins were compared in a t-test versus a large dataset of similar experiments
972 consisting of non-related baits. Proteins not present in the background list or highly enriched
973 versus the large dataset were kept as significant set. Thresholds used are NSAF ratio bait/large
974 dataset ≥ 10 , and $-\log(p\text{-value}) \geq 10$. In this case, 1 peptide identifications were retained,
975 otherwise the small TPC subunit LOLITA would have fallen out of the data. The significant
976 set can be found in Supplemental Table 6.

977 For comparison of the different PBLs versus GSrhino pull-down samples, a MaxQuant search
978 was performed on all relevant TPLATE raw data together. Since LC-MSMS analysis is done
979 the same for the GSrhino as for the Streptavidin pull downs, it's also possible to include
980 matching between runs. Next, resulting iBAQ values were used for comparison of the
981 abundance of the identified proteins amongst the different TPLATE samples. For
982 completeness, one peptide identifications were allowed, in order to also obtain iBAQ values
983 for the one peptide identifications. The complete set of significant proteins as determined by

984 previous analysis, for the PBLs and for CGSrhino, as described, with their iBAQ values can be
985 found in Supplemental Table 6. In Figure 5, a subset of relevant endocytosis related proteins is
986 presented.

987 In order to compare TPLATE-linkerTurboID with different incubation times and at different
988 temperatures, triplicate Streptavidin pull-downs were performed with TPLATE-linkerTurboID
989 and GFP-linkerTurboID at 25 degrees with different incubation times with 50µM biotin.
990 Analysis to determine the significant identifications in each TPLATE-linkerTurboID set versus
991 the respective GFP-linkerTurboID control was done as described before. Significant lists can
992 be found in Supplemental Table 7. For a direct comparison of the different incubation times
993 and temperatures with TPLATE-linkerTurboID, a MaxQuant search was performed on all
994 relevant TPLATE raw data together, with matching between runs. Next, resulting iBAQ values
995 were used for comparison of the abundance of the identified proteins amongst the different
996 sample sets. Again, for completeness, one peptide identifications were allowed, in order to
997 obtain iBAQ values also for the one peptide identifications. For this comparison between
998 linkerTurboID samples only, both elutions were taken together for all sample sets, for the
999 determination of the significant sets as well as for the comparison of the iBAQ values. The
1000 complete set of significant proteins with their iBAQ values can be found in Supplemental Table
1001 6. In figure 6, a subset of proteins is presented.

1002 For each of the TPC subunits, the identified peptides in the TPLATE-linkerTurboID
1003 replicates were mapped to the protein sequence, see Figure 7. Non-biotinylated and
1004 biotinylated peptides of TPC subunits were mapped to the protein sequence by using the Draw
1005 Map tool in the MSTools package (<http://peterslab.org/MSTools/>) (Kavan and Man, 2011) and
1006 put together using Inkscape v 0.92.4 (www.inkscape.org). Domain annotation of TPC subunits
1007 was retrieved using InterPro protein sequence analysis (<https://www.ebi.ac.uk/interpro/>)
1008 (Mitchell et al., 2018).

1009

1010 SUPPLEMENTAL MATERIALS

1011

1012 Supplemental Figure 1. Overview of available constructs for proximity biotinylation in plants.

1013 Supplemental Figure 2. GFP expression in tomato hairy root cultures produced with rhizogenic
1014 *Agrobacterium*.

1015 Supplemental Figure 3. Characterization of PBL-catalysed proximity labelling in *N.*
1016 *benthamiana*.

1017 Supplemental Figure 4. Biotinylation of BioID increases at elevated growth temperature and
1018 biotin concentration in *Nicotiana benthamiana*.

1019 Supplemental Figure 5. *Trans*-biotinylation within membrane-resident receptor complexes.

1020 Supplemental Figure 6. Different PBL cause different *cis*- and *trans*-biotinylation.

1021 Supplemental Figure 7. *Cis*-biotinylation of TPLATE-linkerBioID increases at higher
1022 concentration of exogenous biotin.

1023 Supplemental Figure 8. Exogenous application of biotin can exceed the binding capacity of
1024 streptavidin beads.

1025 Supplemental Figure 9. The biotin-streptavidin interaction is retained under harsh conditions.

1026 Supplemental Table 1. List of expression vectors used in this study.

1027 Supplemental Table 2. list of primers used.

1028 Supplemental Table 3. Cell cultures expressing different TPLATE-PBLs identifies TPC
1029 subunits with different amount of non-biotinylated peptides.

1030 Supplemental Table 4. Full list of significantly enriched identifications with TPLATE-BioID
1031 versus GFP-BioID at different incubation temperatures for 24 hours with 50 μ M biotin.

1032 Supplemental Table 5. Full list of significantly enriched identifications with TPLATE as bait
1033 using BioID, BioID2, linkerBioID, linkerBioID2, linkerTurboID E1, linkerTurboID E2 and
1034 linkerTurboID E1+E2, versus the respective GFP PBLs.

1035 Supplemental Table 6. Full list of significantly enriched hits with either TPLATE PBLs or
1036 GSRhino PD, including average iBAQ values, normalized versus TPLATE.

1037 Supplemental Table 7. Full list of significantly enriched hits with TPLATE-linkerTurboID,
1038 including average iBAQ values, normalized versus TPLATE, at different incubation times at
1039 25 degrees and 24-hour incubation time at 28 degrees, all with 50 μ M biotin.

1040 Supplemental Table 8.

1041 Supplemental sequences. List of all used PBL sequences.

1042

1043

1044 **ACKNOWLEDGEMENTS**

1045 Part of this work was funded by the European Research Council T-Rex project number 682436
1046 to D.V.D.) and by the National Science Foundation Flanders (FWO; G009415N to D.V.D. and
1047 G.D.J.). T.O. and N.B.A. were funded by the Deutsche Forschungsgemeinschaft (DFG,
1048 German Research Foundation) in frame of the Collaborative Research Center 924
1049 (Sonderforschungsbereich 924, INST 95/1126-2, Project B4). P.N.M. funding in support of
1050 this work was from VR (no. 21679000) and FORMAS Research Councils (no. 22924-000), the

1051 Carl Tryggers Foundation (grant nos 15:336 and 17:317), and start-up grants from IMBB-
1052 FORTH.

1053

1054 **AUTHOR CONTRIBUTIONS**

1055 D.A., N.B.A., C.L., P.V.D., K.Y. J.W., B.K. and A.T. designed and/or performed research.
1056 L.D.V., B.K, F.I., D.E. contributed new analytic tools and analyzed data. P.V.D., A.G., G.D.J.,
1057 T.O., P.M. and D.V.D. designed research, analyzed data and wrote the paper. All authors
1058 contributed to finalizing the manuscript text.

1059

1060 **REFERENCES**

- 1061 Alban, C., Job, D., and Douce, R. (2000). BIOTIN METABOLISM IN PLANTS. *Annu Rev Plant Physiol*
1062 *Plant Mol Biol* *51*, 17-47.
- 1063 Antolin-Llovera, M., Ried, M.K., and Parniske, M. (2014). Cleavage of the SYMBIOSIS RECEPTOR-LIKE
1064 KINASE ectodomain promotes complex formation with Nod factor receptor 5. *Curr Biol* *24*, 422-427.
- 1065 Ashby, A.M., Watson, M.D., Loake, G.J., and Shaw, C.H. (1988). Ti plasmid-specified chemotaxis of
1066 *Agrobacterium tumefaciens* C58C1 toward vir-inducing phenolic compounds and soluble factors
1067 from monocotyledonous and dicotyledonous plants. *J Bacteriol* *170*, 4181-4187.
- 1068 Batsios, P., Meyer, I., and Graf, R. (2016). Proximity-Dependent Biotin Identification (BioID) in
1069 *Dictyostelium Amoebae*. *Methods Enzymol* *569*, 23-42.
- 1070 Beckett, D., Kovaleva, E., and Schatz, P.J. (1999). A minimal peptide substrate in biotin holoenzyme
1071 synthetase-catalyzed biotinylation. *Protein Sci* *8*, 921-929.
- 1072 Binder, A., Lambert, J., Morbitzer, R., Popp, C., Ott, T., Lahaye, T., and Parniske, M. (2014). A Modular
1073 Plasmid Assembly Kit for Multigene Expression, Gene Silencing and Silencing Rescue in Plants. *PLOS*
1074 *ONE* *9*, e88218.
- 1075 Boruc, J., Van den Daele, H., Hollunder, J., Rombauts, S., Mylle, E., Hilson, P., Inze, D., De Veylder, L.,
1076 and Russinova, E. (2010). Functional modules in the Arabidopsis core cell cycle binary protein-
1077 protein interaction network. *Plant Cell* *22*, 1264-1280.
- 1078 Branon, T.C., Bosch, J.A., Sanchez, A.D., Udeshi, N.D., Svinkina, T., Carr, S.A., Feldman, J.L., Perrimon,
1079 N., and Ting, A.Y. (2018). Efficient proximity labeling in living cells and organisms with TurboID. *Nat*
1080 *Biotechnol* *36*, 880-887.
- 1081 Choi-Rhee, E., Schulman, H., and Cronan, J.E. (2004). Promiscuous protein biotinylation by
1082 *Escherichia coli* biotin protein ligase. *Protein Sci* *13*, 3043-3050.
- 1083 Clough, S.J., and Bent, A.F. (1998). Floral dip: a simplified method for *Agrobacterium* -mediated
1084 transformation of *Arabidopsis thaliana*. *The Plant Journal* *16*, 735-743.
- 1085 Conlan, B., Stoll, T., Gorman, J.J., Saur, I., and Rathjen, J.P. (2018). Development of a Rapid in planta
1086 BioID System as a Probe for Plasma Membrane-Associated Immunity Proteins. *Frontiers in plant*
1087 *science* *9*, 1882-1882.
- 1088 Cox, J., Hein, M.Y., Lubner, C.A., Paron, I., Nagaraj, N., and Mann, M. (2014). Accurate proteome-wide
1089 label-free quantification by delayed normalization and maximal peptide ratio extraction, termed
1090 MaxLFQ. *Mol Cell Proteomics* *13*, 2513-2526.
- 1091 Cronan, J.E. (2005). Targeted and proximity-dependent promiscuous protein biotinylation by a
1092 mutant *Escherichia coli* biotin protein ligase. *J Nutr Biochem* *16*, 416-418.
- 1093 Das, P.P., Macharia, M.W., Lin, Q., and Wong, S.-M. (2019). In planta proximity-dependent biotin
1094 identification (BioID) identifies a TMV replication co-chaperone NbSGT1 in the vicinity of 126 kDa
1095 replicase. *Journal of Proteomics* *204*, 103402.

- 1096 Deal, R.B., and Henikoff, S. (2011). The INTACT method for cell type-specific gene expression and
1097 chromatin profiling in *Arabidopsis thaliana*. *Nat Protoc* 6, 56-68.
- 1098 Dingar, D., Kalkat, M., Chan, P.K., Srikumar, T., Bailey, S.D., Tu, W.B., Coyaud, E., Ponzielli, R., Kolyar,
1099 M., Jurisica, I., *et al.* (2015). BioID identifies novel c-MYC interacting partners in cultured cells and
1100 xenograft tumors. *J Proteomics* 118, 95-111.
- 1101 Gadeyne, A., Sanchez-Rodriguez, C., Vanneste, S., Di Rubbo, S., Zauber, H., Vanneste, K., Van Leene,
1102 J., De Winne, N., Eeckhout, D., Persiau, G., *et al.* (2014). The TPLATE adaptor complex drives clathrin-
1103 mediated endocytosis in plants. *Cell* 156, 691-704.
- 1104 Gilles, L.M., Khaled, A., Laffaire, J.B., Chaignon, S., Gendrot, G., Laplaige, J., Berges, H., Beydon, G.,
1105 Bayle, V., Barret, P., *et al.* (2017). Loss of pollen-specific phospholipase NOT LIKE DAD triggers
1106 gynogenesis in maize. *EMBO J* 36, 707-717.
- 1107 Grebe, M., Xu, J., Mobius, W., Ueda, T., Nakano, A., Geuze, H.J., Rook, M.B., and Scheres, B. (2003).
1108 *Arabidopsis* sterol endocytosis involves actin-mediated trafficking via ARA6-positive early
1109 endosomes. *Curr Biol* 13, 1378-1387.
- 1110 Grefen, C., and Blatt, M.R. (2012). A 2in1 cloning system enables ratiometric bimolecular
1111 fluorescence complementation (rBiFC). *Biotechniques* 53, 311-314.
- 1112 Gu, B., Lambert, J.P., Cockburn, K., Gingras, A.C., and Rossant, J. (2017). AIRE is a critical spindle-
1113 associated protein in embryonic stem cells. *Elife* 6.
- 1114 Gupta, G.D., Coyaud, E., Goncalves, J., Mojarad, B.A., Liu, Y., Wu, Q., Gheiratmand, L., Comartin, D.,
1115 Tkach, J.M., Cheung, S.W., *et al.* (2015). A Dynamic Protein Interaction Landscape of the Human
1116 Centrosome-Cilium Interface. *Cell* 163, 1484-1499.
- 1117 Harvey, J.J.W., Lincoln, J.E., and Gilchrist, D.G. (2008). Programmed cell death suppression in
1118 transformed plant tissue by tomato cDNAs identified from an *Agrobacterium rhizogenes*-based
1119 functional screen. *Molecular Genetics and Genomics* 279, 509-521.
- 1120 Herberich, E., Sikorski, J., and Hothorn, T. (2010). A robust procedure for comparing multiple means
1121 under heteroscedasticity in unbalanced designs. *PLoS One* 5, e9788.
- 1122 Houbaert, A., Zhang, C., Tiwari, M., Wang, K., de Marcos Serrano, A., Savatin, D.V., Urs, M.J.,
1123 Zhiponova, M.K., Gudesblat, G.E., Vanhoutte, I., *et al.* (2018). POLAR-guided signalling complex
1124 assembly and localization drive asymmetric cell division. *Nature* 563, 574-578.
- 1125 Kajala, K., Coil, D.A., and Brady, S.M. (2014). Draft Genome Sequence of *Rhizobium rhizogenes* Strain
1126 ATCC 15834. *Genome Announc* 2.
- 1127 Karimi, M., Bleys, A., Vanderhaeghen, R., and Hilson, P. (2007a). Building Blocks for Plant Gene
1128 Assembly. 145, 1183-1191.
- 1129 Karimi, M., Bleys, A., Vanderhaeghen, R., and Hilson, P. (2007b). Building blocks for plant gene
1130 assembly. *Plant Physiol* 145, 1183-1191.
- 1131 Karimi, M., De Meyer, B., and Hilson, P. (2005). Modular cloning in plant cells. *Trends Plant Sci* 10,
1132 103-105.
- 1133 Kavan, D., and Man, P. (2011). MStools—Web based application for visualization and presentation
1134 of HXMS data. *International Journal of Mass Spectrometry* 302, 53-58.
- 1135 Khan, M., Youn, J.-Y., Gingras, A.-C., Subramaniam, R., and Desveaux, D. (2018). In planta proximity
1136 dependent biotin identification (BioID). *Scientific Reports* 8, 9212.
- 1137 Kim, D.I., Birendra, K.C., Zhu, W., Motamedchaboki, K., Doye, V., and Roux, K.J. (2014). Probing
1138 nuclear pore complex architecture with proximity-dependent biotinylation. *Proc Natl Acad Sci U S A*
1139 111, E2453-2461.
- 1140 Kim, D.I., Cutler, J.A., Na, C.H., Reckel, S., Renuse, S., Madugundu, A.K., Tahir, R., Goldschmidt, H.L.,
1141 Reddy, K.L., Haganir, R.L., *et al.* (2018). BioSITE: A Method for Direct Detection and Quantitation of
1142 Site-Specific Biotinylation. *J Proteome Res* 17, 759-769.
- 1143 Kim, D.I., Jensen, S.C., Noble, K.A., Kc, B., Roux, K.H., Motamedchaboki, K., and Roux, K.J. (2016). An
1144 improved smaller biotin ligase for BioID proximity labeling. *Mol Biol Cell* 27, 1188-1196.
- 1145 Kim, D.I., and Roux, K.J. (2016). Filling the Void: Proximity-Based Labeling of Proteins in Living Cells.
1146 *Trends Cell Biol* 26, 804-817.

- 1147 Kim, T.-W., Park, C.H., Hsu, C.-C., Zhu, J.-Y., Hsiao, Y., Branon, T., Xu, S.-L., Ting, A.Y., and Wang, Z.-Y.
1148 (2019). Application of TurboID-mediated proximity labeling for mapping a GSK3 kinase signaling
1149 network in Arabidopsis. *636324*.
- 1150 Korbei, B., Moulinier-Anzola, J., De-Araujo, L., Lucyshyn, D., Retzer, K., Khan, M.A., and Luschnig, C.
1151 (2013). Arabidopsis TOL proteins act as gatekeepers for vacuolar sorting of PIN2 plasma membrane
1152 protein. *Curr Biol* *23*, 2500-2505.
- 1153 Kwon, K., and Beckett, D. (2000). Function of a conserved sequence motif in biotin holoenzyme
1154 synthetases. *Protein Sci* *9*, 1530-1539.
- 1155 Law, A.H., Chow, C.M., and Jiang, L. (2012). Secretory carrier membrane proteins. *Protoplasma* *249*,
1156 269-283.
- 1157 Legland, D., Arganda-Carreras, I., and Andrey, P. (2016). MorphoLibJ: integrated library and plugins
1158 for mathematical morphology with ImageJ. *Bioinformatics (Oxford, England)* *32*, 3532-3534.
- 1159 Leitner, J., Petrášek, J., Tomanov, K., Retzer, K., Pařezová, M., Korbei, B., Bachmair, A., Zařímalová,
1160 E., and Luschnig, C. (2012). Lysine⁶³-linked ubiquitylation of PIN2 auxin carrier protein
1161 governs hormonally controlled adaptation of *Arabidopsis* root growth. *Proceedings of*
1162 *the National Academy of Sciences* *109*, 8322-8327.
- 1163 Leys, C., Ley, C., Klein, O., Bernard, P., and Licata, L. (2013). Detecting outliers: Do not use standard
1164 deviation around the mean, use absolute deviation around the median. *J Exp Soc Psychol* *49*, 764-
1165 766.
- 1166 Lin, Q., Zhou, Z., Luo, W., Fang, M., Li, M., and Li, H. (2017). Screening of Proximal and Interacting
1167 Proteins in Rice Protoplasts by Proximity-Dependent Biotinylation. *Front Plant Sci* *8*, 749.
- 1168 Madsen, E.B., Antolin-Llovera, M., Grossmann, C., Ye, J., Vieweg, S., Broghammer, A., Krusell, L.,
1169 Radutoiu, S., Jensen, O.N., Stougaard, J., *et al.* (2011). Autophosphorylation is essential for the in
1170 vivo function of the *Lotus japonicus* Nod factor receptor 1 and receptor-mediated signalling in
1171 cooperation with Nod factor receptor 5. *Plant J* *65*, 404-417.
- 1172 Mair, A., Xu, S.L., Branon, T.C., Ting, A.Y., and Bergmann, D.C. (2019). Proximity labeling of protein
1173 complexes and cell-type-specific organellar proteomes in Arabidopsis enabled by TurboID. *Elife* *8*.
- 1174 Mitchell, A.L., Attwood, T.K., Babbitt, P.C., Blum, M., Bork, P., Bridge, A., Brown, S.D., Chang, H.-Y.,
1175 El-Gebali, S., Fraser, M.I., *et al.* (2018). InterPro in 2019: improving coverage, classification and
1176 access to protein sequence annotations. *Nucleic Acids Research* *47*, D351-D360.
- 1177 Moschou, P.N., Gutierrez-Beltran, E., Bozhkov, P.V., and Smertenko, A. (2016). Separase Promotes
1178 Microtubule Polymerization by Activating CENP-E-Related Kinesin Kin7. *Dev Cell* *37*, 350-361.
- 1179 Moulinier-Anzola, J., Schwihla, M., De-Araujo, L., Artner, C., Jorg, L., Konstantinova, N., Luschnig, C.,
1180 and Korbei, B. (2020). TOLs Function as Ubiquitin Receptors in the Early Steps of the ESCRT Pathway
1181 in Higher Plants. *Mol Plant*.
- 1182 Murashige, T., and Skoog, F. (1962). A Revised Medium for Rapid Growth and Bio Assays with
1183 Tobacco Tissue Cultures. *Physiologia Plantarum* *15*, 473-497.
- 1184 Mylle, E., Codreanu, M.-C., Boruc, J., and Russinova, E.J.P.M. (2013). Emission spectra profiling of
1185 fluorescent proteins in living plant cells. *9*, 10.
- 1186 Nelissen, H., Eeckhout, D., Demuyne, K., Persiau, G., Walton, A., van Bel, M., Vervoort, M.,
1187 Candaele, J., De Block, J., Aesaert, S., *et al.* (2015). Dynamic Changes in ANGUSTIFOLIA3 Complex
1188 Composition Reveal a Growth Regulatory Mechanism in the Maize Leaf. *Plant Cell* *27*, 1605-1619.
- 1189 Opitz, N., Schmitt, K., Hofer-Pretz, V., Neumann, B., Krebber, H., Braus, G.H., and Valerius, O.
1190 (2017a). Capturing the Asc1p/Receptor for Activated C Kinase 1 (RACK1) Microenvironment at the
1191 Head Region of the 40S Ribosome with Quantitative BioID in Yeast. *Molecular & Cellular Proteomics*
1192 *16*, 2199-2218.
- 1193 Opitz, N., Schmitt, K., Hofer-Pretz, V., Neumann, B., Krebber, H., Braus, G.H., and Valerius, O.
1194 (2017b). Capturing the Asc1p/Receptor for Activated C Kinase 1 (RACK1) Microenvironment at the
1195 Head Region of the 40S Ribosome with Quantitative BioID in Yeast. *Mol Cell Proteomics* *16*, 2199-
1196 2218.

1197 Patron, N.J., Orzaez, D., Marillonnet, S., Warzecha, H., Matthewman, C., Youles, M., Raitskin, O.,
1198 Leveau, A., Farre, G., Rogers, C., *et al.* (2015). Standards for plant synthetic biology: a common
1199 syntax for exchange of DNA parts. *New Phytol* 208, 13-19.

1200 Pirner, H.M., and Stolz, J. (2006). Biotin sensing in *Saccharomyces cerevisiae* is mediated by a
1201 conserved DNA element and requires the activity of biotin-protein ligase. *Journal of Biological*
1202 *Chemistry* 281, 12381-12389.

1203 Ried, M.K., Antolin-Llovera, M., and Parniske, M. (2014). Spontaneous symbiotic reprogramming of
1204 plant roots triggered by receptor-like kinases. *Elife* 3.

1205 Roux, K.J., Kim, D.I., Raida, M., and Burke, B. (2012). A promiscuous biotin ligase fusion protein
1206 identifies proximal and interacting proteins in mammalian cells. *J Cell Biol* 196, 801-810.

1207 Schiapparelli, L.M., McClatchy, D.B., Liu, H.H., Sharma, P., Yates, J.R., 3rd, and Cline, H.T. (2014).
1208 Direct detection of biotinylated proteins by mass spectrometry. *J Proteome Res* 13, 3966-3978.

1209 Schwessinger, B., Roux, M., Kadota, Y., Ntoukakis, V., Sklenar, J., Jones, A., and Zipfel, C. (2011).
1210 Phosphorylation-Dependent Differential Regulation of Plant Growth, Cell Death, and Innate
1211 Immunity by the Regulatory Receptor-Like Kinase BAK1. *PLOS Genetics* 7, e1002046.

1212 Tyanova, S., Temu, T., and Cox, J. (2016a). The MaxQuant computational platform for mass
1213 spectrometry-based shotgun proteomics. *Nat Protoc* 11, 2301-2319.

1214 Tyanova, S., Temu, T., Sinitcyn, P., Carlson, A., Hein, M.Y., Geiger, T., Mann, M., and Cox, J. (2016b).
1215 The Perseus computational platform for comprehensive analysis of (prote)omics data. *Nat Methods*
1216 13, 731-740.

1217 Van Damme, D., Coutuer, S., De Rycke, R., Bouget, F.-Y., Inzé, D., and Geelen, D. (2006). Somatic
1218 Cytokinesis and Pollen Maturation in *Arabidopsis* Depend on TPLATE, Which Has
1219 Domains Similar to Coat Proteins. *18*, 3502-3518.

1220 Van Leene, J., Han, C., Gadeyne, A., Eeckhout, D., Matthijs, C., Cannoot, B., De Winne, N., Persiau, G.,
1221 Van De Slijke, E., Van de Cotte, B., *et al.* (2019). Capturing the phosphorylation and protein
1222 interaction landscape of the plant TOR kinase. *Nat Plants* 5, 316-327.

1223 Van Leene, J., Stals, H., Eeckhout, D., Persiau, G., Van De Slijke, E., Van Isterdael, G., De Clercq, A.,
1224 Bonnet, E., Laukens, K., Remmerie, N., *et al.* (2007). A tandem affinity purification-based technology
1225 platform to study the cell cycle interactome in *Arabidopsis thaliana*. *Mol Cell Proteomics* 6, 1226-
1226 1238.

1227 van Steensel, B., and Henikoff, S. (2000). Identification of in vivo DNA targets of chromatin proteins
1228 using tethered dam methyltransferase. *Nat Biotechnol* 18, 424-428.

1229 Varnaite, R., and MacNeill, S.A. (2016). Meet the neighbors: Mapping local protein interactomes by
1230 proximity-dependent labeling with BioID. *Proteomics* 16, 2503-2518.

1231 Wong, J., Nadziejka, M., Madsen, L.H., Bucherl, C.A., Dam, S., Sandal, N.N., Couto, D., Derbyshire, P.,
1232 Uldum-Berentsen, M., Schroeder, S., *et al.* (2019). A *Lotus japonicus* cytoplasmic kinase connects
1233 Nod factor perception by the NFR5 LysM receptor to nodulation. *Proc Natl Acad Sci U S A*.

1234 Youn, J.Y., Dunham, W.H., Hong, S.J., Knight, J.D.R., Bashkurov, M., Chen, G.I., Bagci, H., Rathod, B.,
1235 MacLeod, G., Eng, S.W.M., *et al.* (2018). High-Density Proximity Mapping Reveals the Subcellular
1236 Organization of mRNA-Associated Granules and Bodies. *Mol Cell* 69, 517-532.e511.

1237 Zhang, Y., Song, G., Lal, N.K., Nagalakshmi, U., Li, Y., Zheng, W., Huang, P.J., Branon, T.C., Ting, A.Y.,
1238 Walley, J.W., *et al.* (2019). TurboID-based proximity labeling reveals that UBR7 is a regulator of N
1239 NLR immune receptor-mediated immunity. *Nat Commun* 10, 3252.

1240

1241

1242

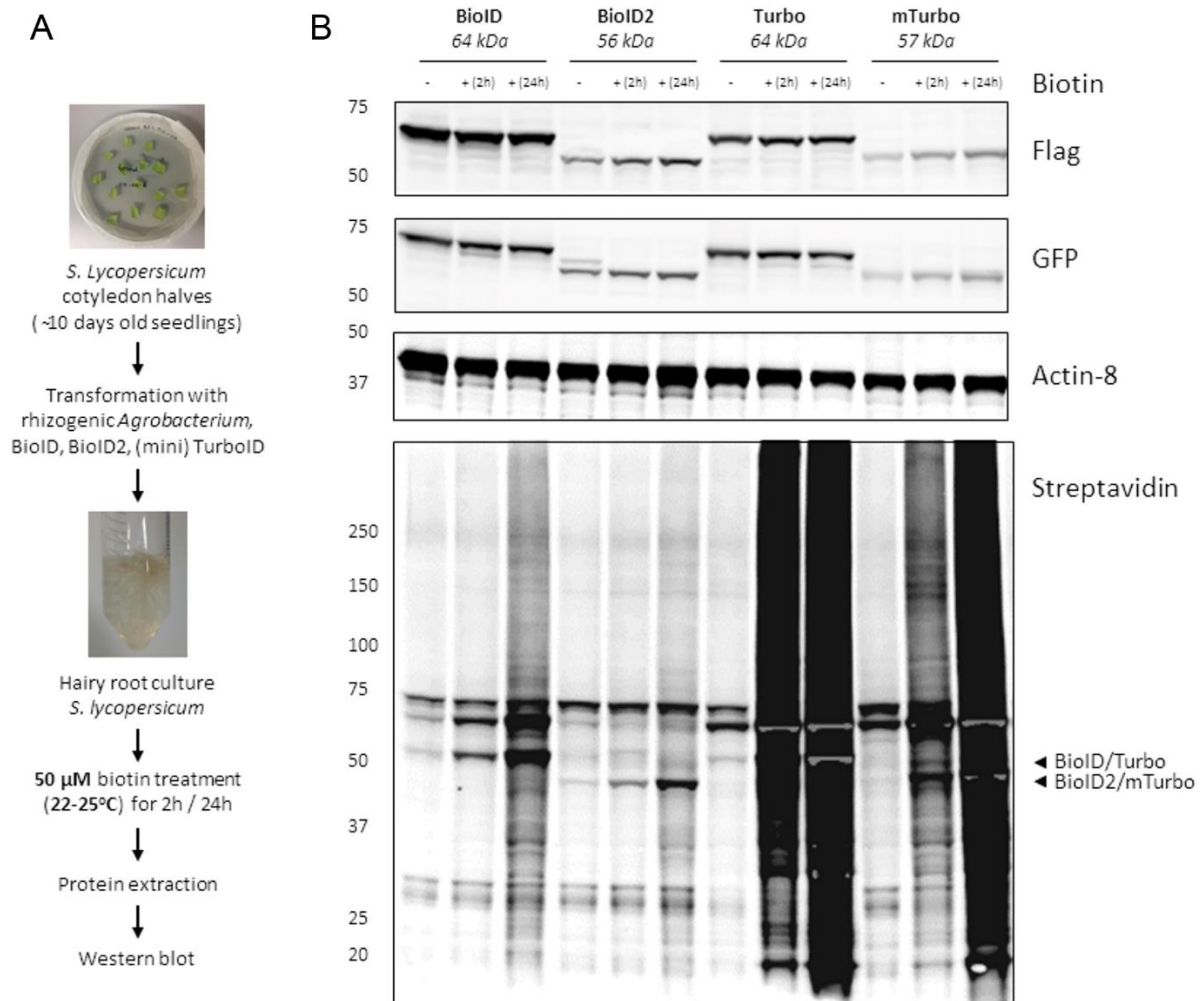
1243

1244

1245

1246 **FIGURES and FIGURE LEGENDS**

1247



1248

1249 **Figure 1. Characterization of enzyme-catalysed proximity labelling in hairy root cultures.**

1250 (A) Experimental setup. (B) Comparison of biotinylation activity in four PBL-expressing hairy

1251 root cultures. Addition of 50 μ M exogenous biotin to two-weeks old hairy root cultures for 2

1252 or 24 h was used for labelling. Arrowheads indicate the expected size of the *cis*-biotinylation

1253 signal. (B) Comparison of biotinylation activity in four PBL hairy root cultures from wild-type

1254 tomato expressing eGFP- BioID-Flag (~66 kDa), eGFP-BioID2-Flag (~56 kDa), eGFP-Turbo-

1255 Flag (~64 kDa) and eGFP-miniTurbo-Flag (~57 kDa). Gray regions in intense black areas

1256 represent saturation of the streptavidin-s680 signal and is most prominent in case of self-

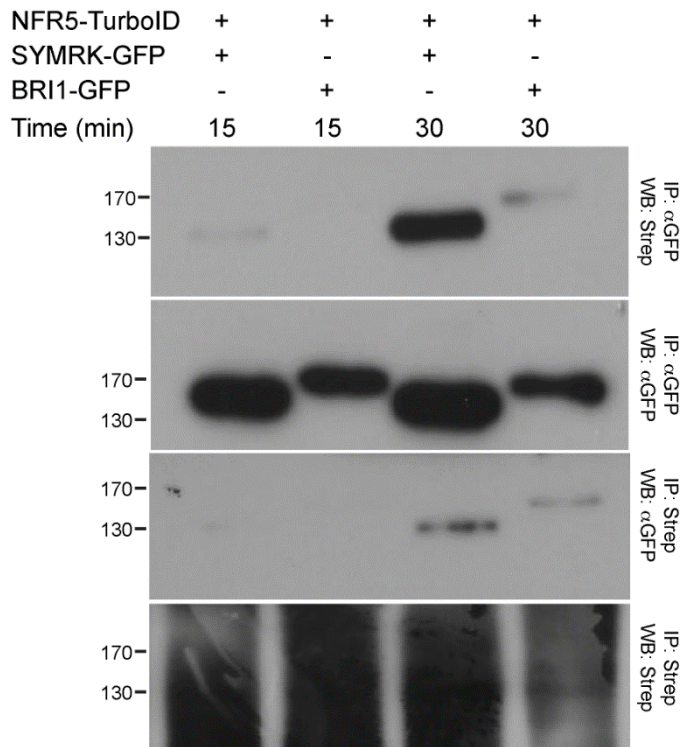
1257 biotinylation activity. This is a representative experiment repeated twice and two independent

1258 root cultures were analyzed per combination.

1259

1260

1261



1262

1263

1264 **Figure 2. NFR5-TurboID shows strong biotinylation of known interactor SymRK-GFP.**

1265 Pairwise combination of NFR5-TurboID (120 kDa) with either SYMRK-GFP (150 kDa) or
1266 BRI1-GFP (157 kDa) using transient expression in *N. benthamiana* leaves allowed time-
1267 dependent and prevalent biotinylation of SYMRK. 50 μM biotin was applied for 15 or 30 min.

1268 IP= immunoprecipitation; WB= Western Blot; Strep= Streptavidin.

1269

1270

1271

1272

1273

1274

1275

1276

1277

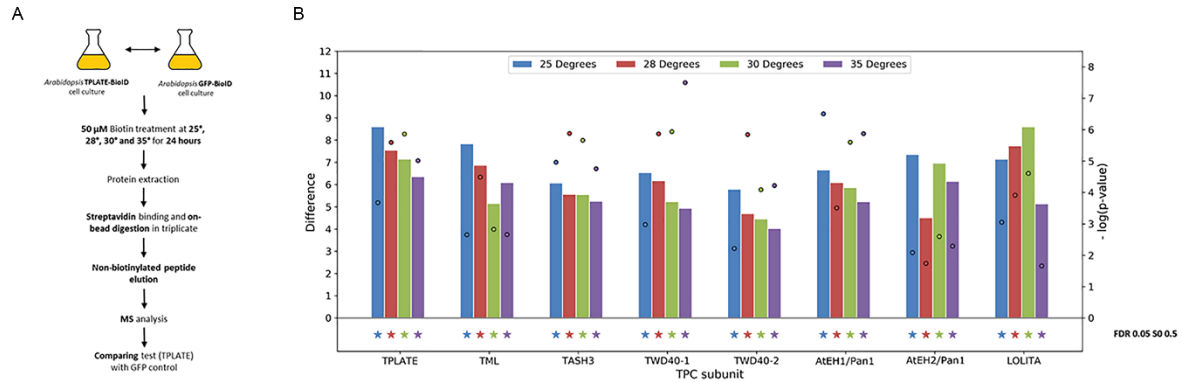
1278

1279

1280

1281

1282



1283

1284 **Figure 3. Detection of TPC subunits with TPLATE-BioID is optimal at 28° C.** (A)

1285 Experimental setup to look for enriched TPC subunits in biotin treated transformed Arabidopsis

1286 cell cultures. Cell cultures were incubated with 50 μ M biotin at 25°-35°C for 24 h before

1287 harvesting. (B) Comparison of the enrichment of the TPC subunits in the TPLATE-BioID

1288 samples at different temperatures compared to their respective GFP-BioID controls. Difference

1289 (bar charts) and $-\log(p\text{-value})$ (dots) are derived from t-tests in Perseus software, using the

1290 average LFQ intensities of 3 technical replicates of TPLATE-BioID versus 3 technical

1291 replicates of GFP-BioID at similar temperature. All TPC subunits are detected at all 4

1292 temperatures without major differences and all are significantly enriched with TPLATE-BioID

1293 (denoted by stars), as determined by permutation based FDR, with cut-offs FDR=0.05 and

1294 S0=0.5. The full list of significantly enriched identifications with TPLATE-BioID at all tested

1295 temperatures can be found in Supplemental Table 4.

1296

1297

1298

1299

1300

1301

1302

1303

1304

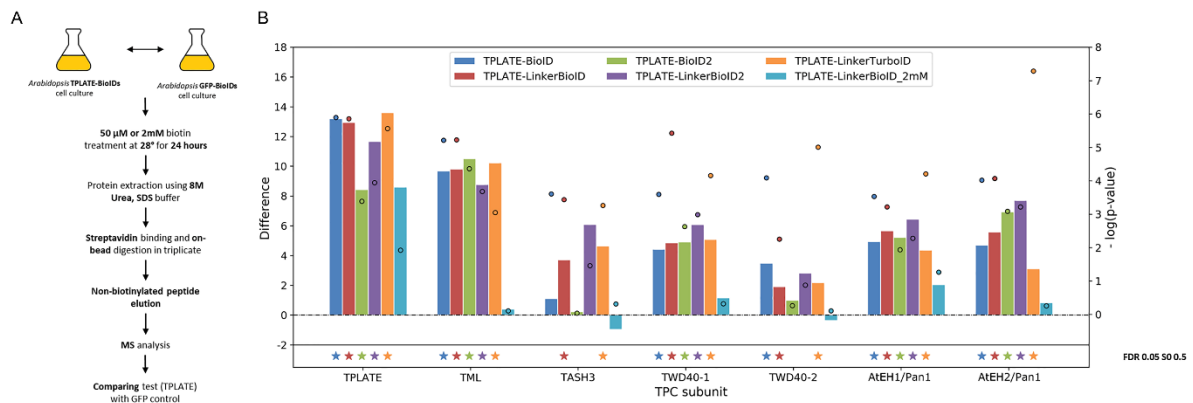
1305

1306

1307

1308

1309



1310

1311 **Figure 4. Different TPLATE-PBLs affect biotinylation of TPC subunits differently. (A)**

1312 Experimental setup. Cell cultures were incubated with 50 μ M biotin at 28° C for 24 h before

1313 harvesting. Protein extraction was performed under harsh conditions to exclude false positives

1314 (B) Comparison of the enrichment of the TPC subunits with different TPLATE-PBLs versus

1315 their respective GFP-PBLs at 28° C. Difference (bar charts) and $-\log(p\text{-value})$ (dots) are

1316 derived from t-tests in Perseus software, using LFQ intensities of 3 technical replicates of the

1317 test compared to 3 replicates of the respective control. The stars below the graph denote that

1318 proteins were found significantly different to the control by permutation based FDR, with cut-

1319 offs $FDR = 0.05$ and $S0 = 0.5$. The full list of significantly enriched identifications with

1320 different TPLATE PBLs at 28 degrees can be found in Supplemental Table 5.

1321

1322

1323

1324

1325

1326

1327

1328

1329

1330

1331

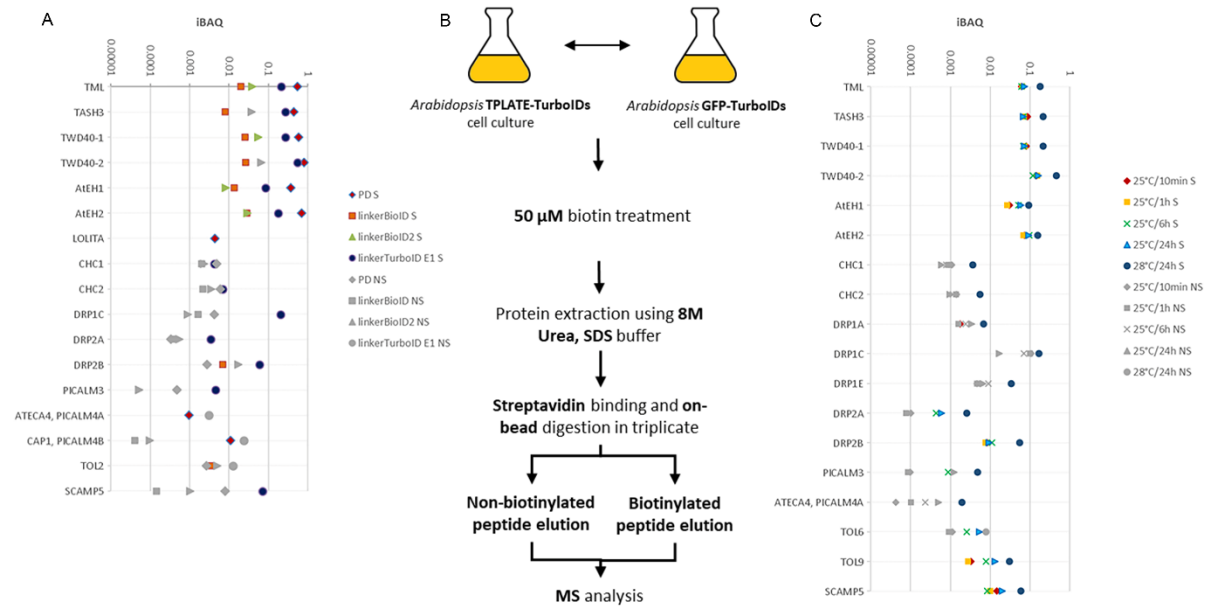
1332

1333

1334

1335

1336



1337

1338 **Figure 5. Comparing identification of a subset of proteins co-purified with TPLATE**
 1339 **using GSRhino pull down (PD), linkerBioID, LinkerBioID2 or LinkerTurboID.**

1340 (A) Pull down and proximity biotinylation comparison of a selection of TPLATE interactors.

1341 Experiments were performed in triplicate, using TPLATE as bait. Per set of experiments,

1342 MaxQuant iBAQ values, which are the summed intensity values divided by the number of

1343 theoretical peptides were calculated and normalized versus the bait in order to compare the

1344 relative abundance of the proteins between the four different approaches. Proteins that were

1345 identified significantly (S) in either method are represented with a colored shape. Proteins that

1346 were identified below the significance threshold (NS) for a given method are indicated with

1347 grey shapes. (B) Schematic overview of the experimental setup to detect biotinylated and non-

1348 biotinylated peptides. Following on-bead digestion, non-biotinylated and biotinylated peptides

1349 were separately analyzed using sequential elutions and all identified peptides were used for MS

1350 analysis. (C) Overview of a subset of the identified interactors, color coded according to their

1351 statistical significance in the different experiments (S=Significant, NS=Not significant) by

1352 combining MS data from both elution fractions. Arabidopsis cell cultures expressing TPLATE-

1353 linkerTurboID were grown at 25 degrees and supplemented with exogenous biotin for 10min,

1354 6hours or 24hrs. Results were compared to the experiment from panel A where the culture was

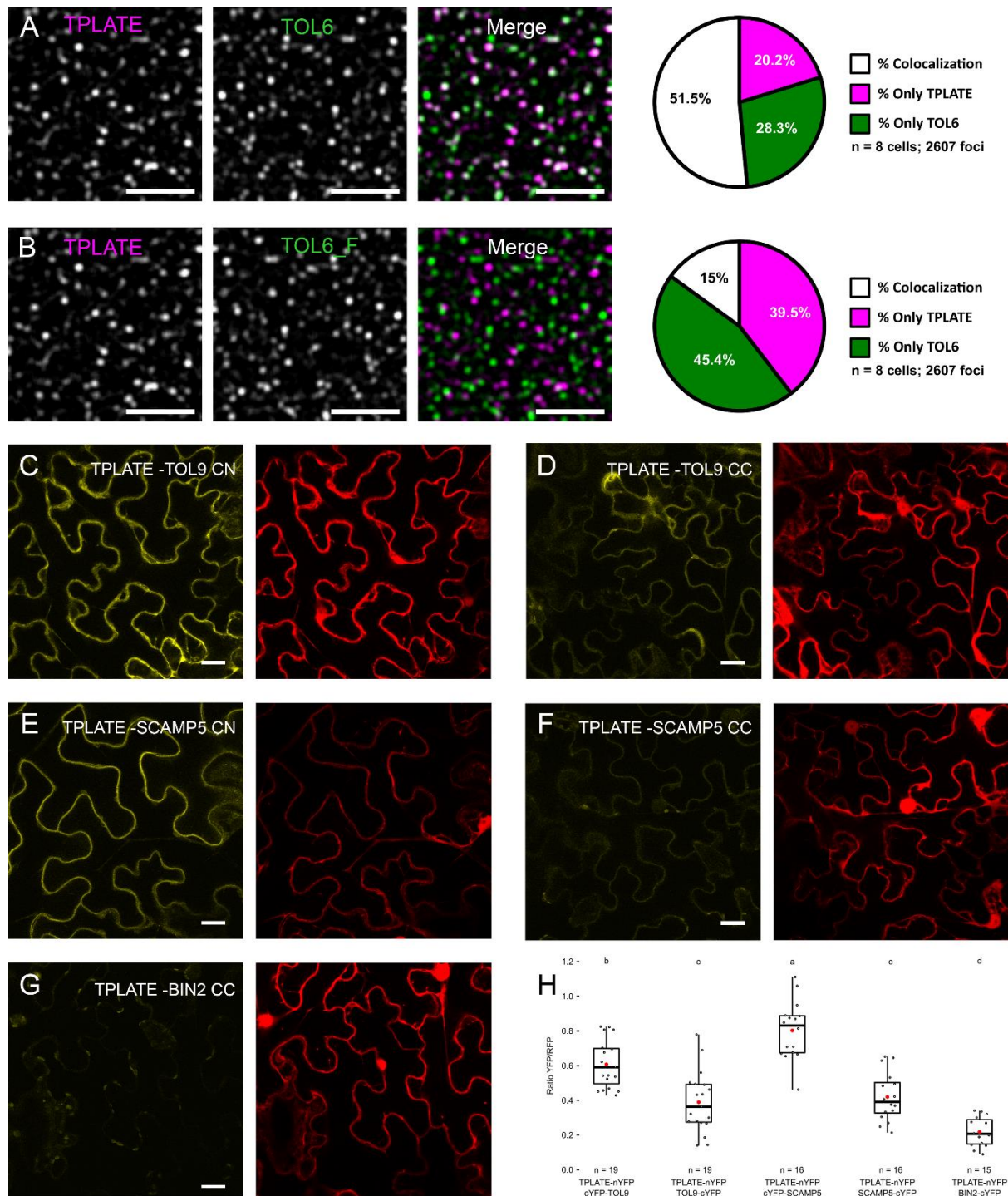
1355 grown at 28 degrees in the presence of biotin for 24hrs. The complete list of significantly

1356 enriched identifications of the experiments shown in panel A and C, including their normalized

1357 average iBAQ values, can be found in Supplemental Table 6 and 7.

1358

1359

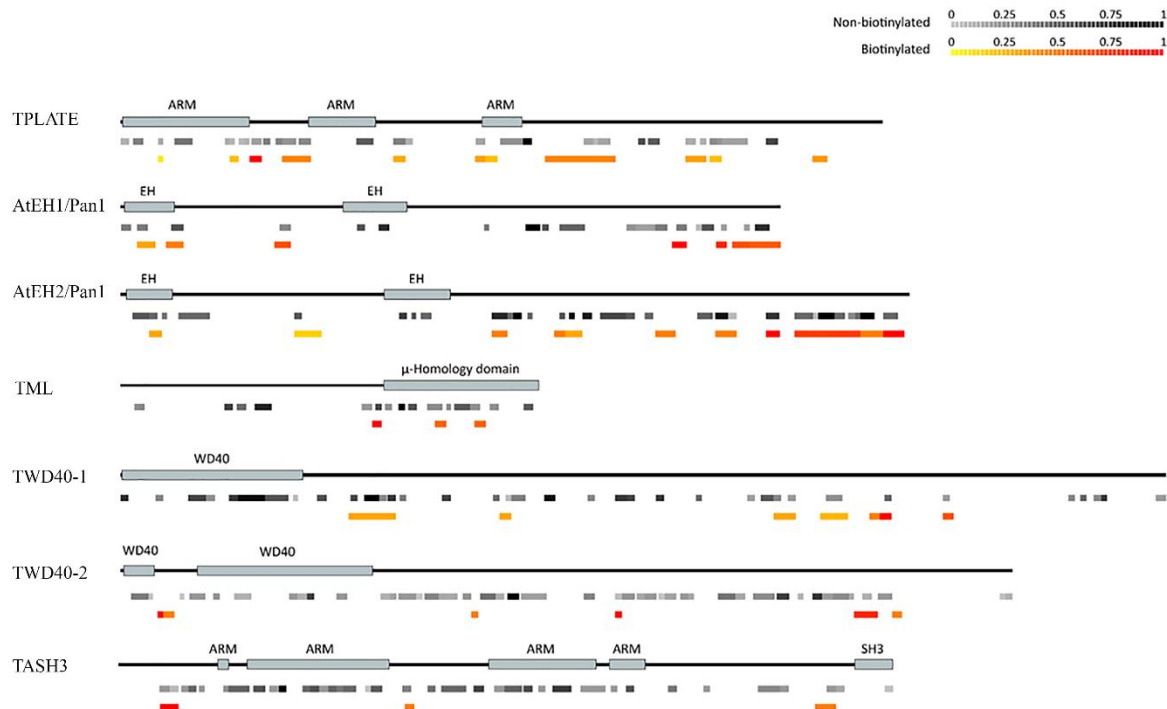


1360

1361 **Figure 6. TOL6, TOL9 and SCAMP5 can be confirmed as novel TPC interactors.**

1362 (A and B) Representative spinning disc dual-color images and corresponding quantification of
 1363 colocalization (%) between TPLATE and TOL6. TPLATE-TagRFP endocytic foci at the PM
 1364 were compared with TOL6-Venus foci (A) as well as horizontally flipped TOL6-Venus
 1365 (TOL6_F) channel images as control (B). Eight movies from three individual plants, and in
 1366 total 2607 foci were analyzed. (C to H) Ratiometric BiFC analysis confirming the interaction
 1367 of TOL9 (C and D) and SCAMP5 (E and F) with TPLATE. BIN2 (G) was used as a control.

1368 CC and CN refer to the orientation of the nYFP and cYFP, N-terminal cYFP is CN and C-
1369 terminal cYFP is annotated as CC. (H) Box plot and Jitter box representation of the
1370 quantification of the YFP/RFP fluorescence ratios ($n \geq 15$). The black line represents the median
1371 and the diamonds represent the mean. Letters above the plots indicate statistical significance
1372 using a Welch-corrected ANOVA to account for heteroscedasticity. Scale bars represent 5 μm
1373 (A and B) or 20 μm (C to G).
1374



1375
1376 **Figure 7. Mapping of biotinylated versus non-biotinylated peptides reveals differential**
1377 **proximity/accessibility of specific TPC subunit domains.** Schematic representation of seven
1378 TPC subunits and their domains. Identified peptides, color-coded according to their abundance
1379 (in grey for non-biotinylated peptides and from yellow to red for biotinylated peptides), are
1380 mapped onto them.

1381
1382
1383
1384
1385
1386
1387